Title: Investigating the developmental onset of regenerative potential in the annelid *Capitella teleta*

Authors: Alicia A. Boyd, Elaine C. Seaver

Whitney Laboratory for Marine Bioscience, University of Florida

Corresponding author: Elaine C. Seaver (seaver@whitney.ufl.edu)

Keywords: regeneration, cell division, larva, *vasa*, metamorphosis

Abstract:

An animal's ability to regrow lost tissues or structures can vary greatly during its life cycle. The annelid *Capitella teleta* exhibits posterior, but not anterior, regeneration as juveniles and adults. In contrast, embryos display only limited replacement of specific tissues. To investigate when during development *C. teleta* becomes capable of regeneration, we assessed the extent to which larvae can regenerate. We hypothesized that larvae exhibit intermediate regeneration potential and demonstrate some features of juvenile regeneration, but do not successfully replace all lost structures. Both anterior and posterior regeneration potential of larvae were evaluated following amputation. Wound sites were analyzed for re-epithelialization, cell proliferation by EdU incorporation, stem cell and differentiation marker expression by in situ hybridization, presence of neurites and muscle fibers by immunohistochemistry and phalloidin staining respectively, and regrowth of structures. Wound healing occurred within 6 hours of amputation for both anterior and posterior amputations. Cell proliferation at both wound sites was observed for up to 7 days following amputation. In addition, the stem cell marker *vasa* was expressed at anterior and posterior wound sites. However, growth of new tissue was observed only in posterior amputations. Neurites from the ventral nerve cord were also observed at posterior wound sites. *De novo ash* expression in the ectoderm of anterior wound sites indicated neuronal cell specification, although the absence of *elav* expression indicated an inability to progress to neuronal differentiation. In rare instances, cilia and eyes reformed. Both amputations induced expanded expression of the myogenesis gene *MyoD* in pre-existing tissues. Our results indicate that amputated larvae complete early, but not late, stages of regeneration, indicating a gradual acquisition of regenerative ability in *C. teleta.* Furthermore, amputated larvae can metamorphose into burrowing juveniles, including those missing brain and anterior sensory structures. To our knowledge, this is the first study to assess regenerative potential of annelid larvae.

1. Introduction

Regeneration is the replacement of tissues or structures after injury or amputation. The ability to regenerate lost tissues varies throughout the animal kingdom (Alvarado, 2000). For example, animals such as planarians and hydra can completely reform any lost structure with hardly any restriction (i.e., whole-body regeneration) (Reddien, 2020; Reddy et al., 2020). Other animals have a more restrictive capacity to regenerate and reform only specific structures, such as limbs in crustaceans (Alwes et al., 2016) and amphibians (Brockes, 1997; Byrnes, 1904; Singer, 1954). Finally, some animals, like the leech, display almost no regenerative capabilities following bisection (Özpolat & Bely, 2016). Here, we briefly review differences in regeneration potential across animal life cycles and describe the need to more carefully examine regeneration in pre-adult stages. We highlight annelids as a clade with exceptional regeneration diversity and introduce *Capitella teleta* as a prime candidate to examine how regeneration changes during the life cycle of an indirect developer.

Most published surveys of regeneration ability focus on adult stages, while few studies examine regeneration potential at earlier stages of the life cycle. Several questions emerge when one considers regeneration potential across the life cycle. In animals with a biphasic life cycle, does regeneration ability differ among embryos, larvae, and adults? If so, when in the life cycle is the regeneration program activated – during larval stages or after metamorphosis? Are there conserved trends of increasing or decreasing regeneration abilities across the life cycle? From a developmental perspective, one might expect a trend of decreasing regeneration abilities through the life cycle as embryonic cells become committed to distinct cell types, undergo terminal differentiation, and lose their pluripotency. As a result, there would be progressive loss in the ability to replace tissues (e.g., appendages, nervous system, and heart) (Yun, 2015; Porello et al., 2011; Walters & Zuo, 2013). However, in animals with indirect life cycles, larvae and adults often have distinct tissues, and adult tissue formation requires the retention of progenitors or multipotent stem cells through the larval phase (Peterson et al., 1997). The presence of stem cells in larvae suggests the possibility that animals with indirect development may have greater regeneration potential relative to direct developing species.

The published studies that do examine regeneration in larvae are disproportionately sampled from deuterostomes. From these examples, a complex picture emerges; a single relationship between larval and adult regeneration ability does not explain published observations across species. For example, the *Xenopus* frog (Phipps et al., 2020) has a pattern of regeneration loss similar to what is observed in direct developers: an ability to replace specific tissues (i.e., appendages, heart, brain, lens) as larvae that is lost with maturation (Harrison, 1898). The crinoid, *Antedon rosacea*, is very different such that the larvae exhibit limited ability to regenerate following bisection, but adults are capable of whole-body regeneration (Carnevali, 2006; Carnevali et al., 1993). Furthermore, sea stars exhibit whole-body regeneration during larval, juvenile, and adult stages (Carnevali, 2006). Other animals have a more dynamic change in regenerative ability through their life cycle. *Ciona intestinalis* lacks regenerative abilities as a larva yet exhibits structural regeneration as adults only to progressively lose this ability with advanced age (Jeffery, 2015). A broad understanding of how regeneration ability relates to the life cycle is largely unexplored, and it is critical to sample pre-adult stages in animal taxa with demonstrated regeneration abilities as adults, particularly from protostome lineages.

Annelids are segmented worms that have a wide range of regenerative abilities as adults. Some lack the ability to regenerate following transverse amputation, others regenerate either anterior or posterior

segments only, or even undergo whole-body regeneration (Bely, 2006). A systematic review of annelid regenerative ability revealed that anterior and posterior regeneration are widespread across the phylum, alongside numerous examples of loss of regeneration (Bely, 2006). Furthermore, it is likely that both anterior and posterior regeneration are ancestral for adult annelids (Zattara & Bely, 2016). Although some studies have characterized regeneration during juvenile stages (del Olmo et al., 2021; Kostyuchenko, 2022; Planques et al., 2019), to our knowledge, a broad assessment of larval regenerative potential is lacking for annelids.

Capitella teleta BLAKE ET AL 2009 is an annelid capable of posterior regeneration and has an indirect life cycle (Seaver, 2022). Previous studies hint at changes in the ability of *C. teleta* to replace lost structures across its life cycle. Juvenile and adult worms regenerate following bisection along the main body axis (de Jong & Seaver, 2016; Giani et al., 2011). In contrast, early-stage embryos do not regulate following deletion of individual precursor cells (Pernet et al., 2012) (apart from eye and germline precursor cells (Dannenberg & Seaver, 2018; Yamaguchi et al., 2016)). It is unknown when *C. teleta* gains its regenerative ability, or to what degree larvae might be capable of regeneration.

Following *C. teleta* embryogenesis, a non-feeding lecithotrophic larva forms. Lecithotrophic larvae often have 'abbreviated developmental times' (Vickery et al., 2001), which characterizes the *C. teleta* larval phase of approximately 5 - 6 days in duration. Larvae are characterized by trochal ciliated bands that divide the body into three regions along the anterior–posterior axis: the head, the segmented trunk, and the pygidium. The prototroch separates the head from the trunk and the telotroch separates the trunk from the pygidium (Fig 1A, B) (Seaver et al., 2005). These two ciliary bands are composed of long cilia. A third ciliary band, the neurotroch, runs along the ventral midline of the trunk and is composed of short cilia. Short cilia are also present in the pygidium. Larvae utilize the prototroch and telotroch to swim in the water column, aiding in dispersal.

During larval stages, the adult centralized nervous system, musculature, digestive system, and initial systems mature (Meyer et al., 2015). A previously described staging system uses morphological features to identify nine distinct stages of embryonic (Stages 1-3) and larval development (Stages 4-9) (Seaver et al., 2005). *C. teleta* has a centralized nervous system whose development is initiated in late embryogenesis. A ladder-like ventral nerve cord (VNC) positioned along the midline of the trunk forms and is connected to the brain by a pair of circumoral nerves (Meyer et al., 2015; Seaver et al., 2005). The body wall musculature is organized segmentally with circular and longitudinal muscles, and the first muscle fibers appear at the beginning of larval life (Stage 4). Two pigmented eyes appear at Stage 5 and are located lateral and anterior to the prototroch (Meyer et al., 2015; Yamaguchi et al., 2016). Gut organogenesis becomes visibly pronounced between Stages 6–9. The foregut consists of the mouth, buccal cavity, pharynx (morphogenesis in Stage 7), and esophagus (Boyle & Seaver, 2008; see Fig 1A and Fig 1B). In Stages 8–9, the midgut differentiates, becoming olive green and stereotypically coiled (Fig 1B). Stage 6 larvae have approximately 10 segments, generating one segment a day until there are approximately 13 segments present in Stage 9 larvae (Seaver et al., 2005). Larval development concludes when Stage 9 larvae metamorphose into burrowing juvenile worms (Cohen & Pechenik, 1999; Seaver et al., 2005).

We sought to determine when regeneration potential is initiated during the life history of *C. teleta*. We hypothesized that larvae may have limited regeneration potential distinct from juveniles and adults. We anticipated that larvae would display early stages of regeneration without successfully replacing lost

151 tissues and structures. This would suggest that *C. teleta* acquires its regenerative ability gradually
152 through its life cycle. To test our hypothesis, we developed an amputation protocol for larvae to
153 investigate both anterior and posterior regeneration. We characterized larval responses to amputation
154 by making direct comparisons with regeneration events in juveniles. At the wound site, we documented
155 epithelial wound healing, evaluated cell proliferation by EdU incorporation, analyzed changes in
156 neuronal organization with antibody labeling, and visualized musculature with phalloidin staining. We
157 also conducted *in situ* hybridization experiments to analyze expression of the neuronal specification and
158 differentiation gene markers, *ash1* and *elav*, respectively, as well as examine muscle fate and
159 differentiation through analysis of the *MyoD* gene.

160

161 **2. Materials and Methods**

162 *2.1 Animal Care*

163 As described in previous work (Grassle & Grassle, 1976), a colony of *Capitella teleta* was
164 maintained in the laboratory at 19°C in glass finger bowls containing filtered sea water (FSW) and a thin
165 layer of mud. Using forceps, larvae were dissected from the brood tubes of healthy females. Larvae from
166 a single brood tube develop synchronously and the number of individuals/brood averaged 100 – 250
167 individuals. Brood tubes were maintained in FSW until the desired age for amputation or treatment.

168 *2.2 Amputations*

169 Stage 6 larvae were used for amputation experiments. Larvae were developmentally staged
170 following a standard staging system (Seaver et al., 2005). Stage 6 is characterized by presence of yolk in
171 the anterior portion of the larva, swimming behavior with a positive phototactic response, and lack of
172 chaetae. Prior to amputation, larvae were incubated in 1:1 $MgCl_2$: FSW for 10 minutes to inhibit muscle
173 contraction. Individual larvae were transferred a 60 mm petri dish lid filled with a methyl cellulose
174 solution (0.3 g methyl cellulose in 15 ml filtered sea water) for amputation. Additional methyl cellulose
175 was added as necessary to achieve immobilization. Glass capillary tubes (50 µl, Becton Dickinson and
176 Company) were heated over a flame and pulled into thin, flexible, sharp tips to use as amputation tools.
177 Larvae were amputated with a single continuous, downward motion. Cut sites for anterior amputations
178 and eye amputations were located just posterior to the prototroch, removing the anterior third of the
179 animal (i.e., brain, eyes, and prototroch). Cut sites for posterior amputations were located ~2/3 of the
180 body length posterior to where the width of the trunk decreases and slopes to the pygidium, effectively
181 removing the posterior growth zone, telotroch and pygidium. Following amputation, each individual was
182 visually inspected for correct cut location and complete separation of the two tissue fragments.
183 Amputated larvae were transferred to a 60 mm petri dish containing 1:1 0.37M $MgCl_2$: FSW and
184 incubated for a minimum of 1 hour. Larvae were then washed into FSW containing 60 µg/ml penicillin
185 and 50 µg/ml streptomycin (Sigma-Aldrich Co.) (P/S) and raised at 19°C. P/S FSW was replaced daily, and
186 vitality and swimming behavior were monitored daily. For each amputation experiment, age matched
187 larvae from the same brood tube as experimental animals were raised as uncut controls. In a typical
188 experiment, 40 – 60 individuals from a single brood were amputated. For posterior amputations,
189 amputations were performed on sets of individuals from at least 10 broods, and for anterior

190 amputations, sets of individuals from at least 5 broods were amputated. Both anterior and posterior
191 amputated larvae had high rates of survivorship, ranging from 75% (n= 37/50) to 85% (n=28/33).

192 Two-week-old juveniles were prepared for amputation by incubation in 1:1 $MgCl_2$: FSW for 10
193 minutes. Individual worms were transferred to a platform of black dissecting wax (American Educational
194 Products, Fort Collins, CO, USA) in the lid of a 35 mm plastic dish for amputation in a drop of 1:1 $MgCl_2$:
195 FSW. For eye amputations, worms were amputated immediately anterior to the mouth, removing the
196 eyes and brain. Amputations for posterior regeneration were at the boundary between segment 10 and
197 11. Individual worms were visually inspected for the correct cut site and successful separation before
198 being transferred to a 60 mm petri dish and incubated in 1:1 $MgCl_2$: FSW for a minimum of 1 hour. The
199 juveniles were then washed into FSW and moved to a 60 mm petri dish containing mud and FSW and
200 raised at 19°C for 1 week. For analysis, juvenile worms were sifted from the mud and placed into a petri
201 dish of FSW. Worms were fixed with 4% paraformaldehyde (PFA) in FSW for 30 min before being washed
202 into phosphate-buffered saline (PBS). Fixed juveniles were scored for pigmented eye cells before being
203 processed for antibody labeling.

204 *2.3 Cell Proliferation Assay*

205 Larvae were incubated in EdU (Click-iT EdU Alexa Fluor 488 imaging kit - Invitrogen) diluted in
206 FSW to a final concentration of 3 uM at room temperature for 30 minutes. Larvae were then washed
207 into a 1:1 $MgCl_2$: FSW solution for 10 minutes and then fixed in 4% PFA for 30 minutes. Afterward, they
208 were rinsed into PBS and incubated for 20 minutes at room temperature in PBS + 0.05% Triton-X-100
209 with rocking. The specimens were incubated in the commercially provided EdU reaction buffer for 30
210 minutes, rocking at room temperature. Finally, larvae were washed into PBS and stored at 4°C until
211 further analysis.

212 *2.4 EdU Quantification*

213 Quantification of EdU and DAPI stained cells in uncut and amputated larvae was conducted by
214 importing Z-stacks generated from confocal microscopy (see Microscopy) into ImageJ software. Using
215 DAPI and DIC channels to establish boundaries, each image was cropped around the perimeter of the
216 animal. The channels were split and treated separately to optimize cell counting. The threshold for each
217 channel was adjusted manually to minimize background and enhance distinction of individual cells.
218 Afterward, a mask and watershed application were applied to each channel. The resulting image was
219 divided into three equal sections along the anterior-posterior axis using the Montage to Stack
220 application. The modified images were compiled into 20 slice projections (20 µm total) before being
221 counted automatically by Analyze Particles in the Analyze menu. Each 20 µm Z-stack was counted, with
222 the results automatically summarized via section. Manual inspection eliminated any cells that were
223 counted twice by the software. Results were manually compiled by channel and section for each animal,
224 as well as for each time point. A ratio of EdU stained cells to DAPI stained cells was calculated for each
225 time point from the ImageJ cell count summaries. Averages of each body section (anterior, middle, and
226 posterior) for each time point (uncut controls, 6 hpa, 3dpa, and 5dpa) were calculated separately. Ten
227 randomly selected larvae were scored for each time point and a mean value was calculated for each

body section across individuals. Each body section of uncut controls was compared with corresponding body sections of amputated animals. One-way weighted ANOVA statistical tests were performed using VassarStats (Lowry, 2023) to test for significance between the control and amputation group of interest.

2.5 Antibody labeling and phalloidin staining

Amputated larvae or juveniles were incubated in a 1:1 $MgCl_2$: FSW solution for 10 minutes and fixed in 4% paraformaldehyde in FSW for 30 minutes. Animals were washed several times into PBS to remove fixative and then washed into a PBS + Triton solution (PBT) (0.1% Triton-X-100 for larvae and 0.2% Triton-X-100 for juveniles). Animals were transferred to a 3 well glass depression plate and incubated in a solution of 10% heat inactivated normal goat serum in PBT at room temperature with rocking for 45–60 min. For antibody labeling, the anti-acetylated tubulin antibody (goat anti-mouse, Sigma-Aldrich Co.) was diluted 1:400 in block solution (10% heated treated goat serum in PBT), and incubated with larvae or juveniles at room temperature for 2 hours or overnight at 4°C. Following multiple washes in PBT (4 times in PBT for 30 minutes each), a secondary antibody (goat anti-mouse red 594, Invitrogen) was diluted 1:400 in block solution and added to animals prior to incubation for 2–4 hours rocking at room temperature or overnight at 4°C. The 22C10 antibody (Goat anti-mouse, Developmental Studies Hybridoma bank; 22C10 was deposited to the DSHB by Benzer, S. / Colley, N. (DSHB Hybridoma Product 22C10)) was diluted 1:200 in block solution, added to animals and incubated overnight at 4°C. Following multiple washes in PBT over two hours, the secondary antibody (goat anti-mouse green 488 - Invitrogen) was diluted 1:400 in block solution, added to animals and incubated overnight at 4°C. Following incubation in secondary antibody, larvae were rinsed 2–3 times in PBT and then washed 4 times in PBT for 30 minutes each wash. For phalloidin staining, specimens were incubated in a 1:400 dilution of phalloidin (Alexa Fluor 488 phalloidin, Invitrogen) in PBT. Specimens were incubated on a rocker at room temperature for 45–60 min before being washed twice in PBT for 30 minutes each wash. Animals were cleared in 80% glycerol in PBS with 1 µg/ml Hoechst-33342 (Molecular Probes) overnight prior to imaging.

2.6 Whole mount in situ hybridization

Larvae collected at different time points following amputation were incubated in a 1:1 $MgCl_2$: FSW solution for 10 minutes and then fixed in 4% paraformaldehyde overnight at 4°C. Fixative was removed by multiple rinses in PBS and then larvae were gradually washed into 100% methanol and stored at -20°C. Whole mount in situ hybridization was performed following a previously published protocol (de Jong & Seaver, 2017). DIG-labeled RNA probes were generated with the MegaScript SP6 or T7 Transcription kit (Invitrogen) according to manufacturer instructions. The following probes and their working concentrations were used: *ash1* with 3ng/ul, *MyoD* with 0.5ng/ul, *vasa* with 1ng/ul, and *elav* with 2ng/ul. Animals were hybridized for ~24 – 48 hours with riboprobe at 65°C. Each RNA probe was visualized by exposure to an anti-digoxigenin-alkaline phosphatase conjugate antibody (Roche) prior to exposure to a color reaction solution containing NBT/BCIP (nitro blue tetrazolium chloride/5-bromo-4-chloro-3-indolyphosphate) and visually monitored for optimal development time. For each sample, uncut control larvae were developed for the same duration as experimental, amputated larvae. Color reactions were terminated following washes of PBT followed by a final fixation in 4% PFA in FSW for 30

267 min. Tissue was cleared in 80% glycerol in PBS plus 0.1 ug/ml Hoescht to stain nuclei, and then
268 individuals were placed on microscope slides for analysis and imaging. At least two independent
269 repetitions were performed for each gene.

270 *2.7 Tissue and Cilia Measurements*

271 To measure tissue formation in amputated larvae, confocal images were analyzed using ImageJ
272 software. Multiple measurements were made on each specimen. The nervous system was measured
273 from the cut site to the position most distal from the cut site that contained neurites. Muscle
274 measurements were taken to the position most distal from the cut site that contained phalloidin-
275 positive fibers. Changes in body width were calculated by making two measurements per specimen; the
276 first measurement was taken at the axial level of the mouth, and the second was just posterior to the
277 cut site. Gut measurements were made from the posterior end of the pigmented midgut to the
278 posterior edge of the posterior ectoderm. For anterior amputations, the muscle and nervous system
279 were measured on 6 hpa (n = 8) and 3 dpa (n = 10) larvae. For posterior amputations, the muscle,
280 nervous system, and changes in body width were measured for 6 hpa (n = 7) and 5 dpa (n = 10).
281 Additionally, the posterior edge of the midgut was used as a landmark for measurements in 5 dpa and
282 Stage 9 larvae at 6 hpa (n = 10). One-way weighted ANOVA statistical tests were performed using the
283 *Good Calculators* software (Good calculators, 2023) to test for significance between the uncut control
284 and experimental amputation group of interest.

285 The cilia of larvae were measured using ImageJ software on confocal image projections.
286 Individual labeled cilia of the prototroch, neurotroch, telotroch, and pygidium were traced. Lines
287 resulting from the trace were then measured using the 'measure' tool found under 'Analyze.' At least
288 three cilia for each ciliary band type were measured in a representative individual, and three individuals
289 were measured, resulting in a total of at least nine measurements for each of the prototroch, telotroch,
290 neurotroch and pygidium ciliary lengths. The range of cilia lengths across the nine measurements is
291 reported (see Results).

292 *2.8 Metamorphosis assays*

293 Metamorphosis is rapidly induced in *C. teleta* by exposure to vitamin B supplements (Burns et
294 al., 2014). A single multivitamin (Centrum Men Multivitamin) was dissolved in 200 ml FSW and stored at
295 room temperature. To test whether amputated larvae are capable of successful metamorphosis, uncut,
296 anteriorly amputated, and posteriorly amputated larvae were exposed to the multivitamin solution
297 containing vitamin B. Larvae were placed in a 30mm petri dish in FSW. Most of the FSW was removed
298 from the dish and replaced with 3 ml of the multi-vitamin solution. Animals were incubated in the
299 vitamin solution for 20 - 30 minutes. The multi-vitamin solution was removed by a minimum of three
300 washes with FSW (2 ml/wash), and then animals were individually scored for settlement and
301 metamorphosis. Successful settlement and metamorphosis were defined as cessation of swimming
302 behavior and initiation of burrowing, loss of the prototroch and telotroch ciliary bands, and elongation
303 of the body.

304 *2.9 Microscopy and Imaging Analysis*

Larvae were imaged with a Zeiss 710 confocal microscope using 4x bidirectional and unidirectional scan settings for the green and red lasers. Z-stacks were compiled using ImageJ software (Schindelin et al., 2012). Differential interference contrast microscopy images were captured on a Zeiss AxioSkop II motplus compound microscope (Zeiss) coupled with a SPOT FLEX digital camera (Diagnostic Instruments Inc). Multiple focal planes were merged for DIC images using Helicon Focus software (Helicon Focus 7). Images were cropped and processed for brightness and contrast with Photoshop (Adobe Photoshop 2020) or Illustrator (Adobe Illustrator 2020). Figures were composed in Adobe Illustrator (Adobe Illustrator 2020).

3. Results

3.1 Characteristics of successful regeneration in C. teleta

To characterize larval regenerative potential, we looked to the juvenile posterior regeneration program in *C. teleta* to define features of successful regeneration. *C. teleta* juveniles maintain three conserved sequential stages of posterior regeneration: wound healing, cell proliferation, and differentiation of new tissues (de Jong & Seaver, 2016). Following amputation, juveniles wound heal in 4–6 hours and thereafter form a blastema (Fig 1C) (de Jong & Seaver, 2016). Neuronal projections extend from the VNC into the wound site as early as 2 days post amputation (dpa) (Fig 1D; see also de Jong & Seaver, 2016). In regenerating juveniles, the thickness of the connective nerve decreases dramatically at the point of amputation, with multiple thin neural projections extending from the old VNC tissue into the wound tissue and thereafter into the blastema/new tissue. This change in VNC thickness indicates the position of the cut site. Localized cell proliferation is also observed at the wound site by 2 dpa and persists for several days as new segments form (de Jong & Seaver, 2016). We observed the density of circular and longitudinal muscle fibers decrease abruptly at the wound site at 3 dpa (Fig 1E). Circular and longitudinal muscle fibers are absent between the posterior boundary of the old tissue and phalloidin-positive fibers at the posterior end of the animal. The decrease in muscle fibers spatially align with the decrease in thickness of the connective nerves of the VNC. After approximately 7 days, additional segments are formed that contain organized ganglia, peripheral nerves, circular and longitudinal muscles, digestive tissue and other differentiated tissues (de Jong & Seaver, 2016).

3.2 Amputation responses in larvae and subsequent development

To assess the regenerative potential of *C. teleta* larvae, sites were selected for both anterior and posterior amputations that removed approximately 1/3 of the body (Fig 2A). Initial analysis focused on wound healing, which is identified by presence of a continuous epithelial layer covering the wound site and results from contraction of the severed edges of the body wall. To assess wound healing in amputated larvae, we analyzed Stage 6 larvae fixed at 2 hours post amputation (hpa), 3 hpa, 5 hpa, and 6 hpa for presence of a continuous epithelial layer covering the wound site. Following anterior amputations, we observed consistent wound healing 6 hpa (Fig 2B) (n = 54/54). For posterior amputations, we observed wound healing as early as 2 hpa (n = 3/15); however, in most cases successful wound healing occurred around 6 hpa (Fig 2C) (n = 48/51). In posterior amputations performed on Stage 9 larvae, successful wound healing also occurred by 6 hpa (Fig 2D). Presence of tissue between the posterior edge of the pigmented midgut and the posterior epidermis of most animals indicated wound healing of the mesodermal layer by 6 hpa.

346 Larvae survived multiple days following amputation and continued to develop towards metamorphic
347 competency. Amputated larvae generally had high survivorship (~75-85%) at 5 dpa, with anteriorly
348 amputated animals and posteriorly amputated animals surviving up to 5 dpa and 7 dpa, respectively.
349 Furthermore, amputated larvae continued to develop on schedule relative to uncut animals (Fig 2E, 2F).
350 For example, in posteriorly amputated larvae, chaetae were present in the original tissue by 1 dpa
351 (comparable to Stage 7), pigmentation appeared in the midgut by 2 dpa (comparable to Stage 8), and
352 the midgut became coiled by 3 dpa (comparable to Stage 9). Anteriorly amputated larvae also
353 developed chaetae and a pigmented midgut, but the curvature of midgut—a hallmark of Stage 9 larvae
354 (Boyle & Seaver, 2008; Seaver et al., 2005) was delayed by one day. The growth of anterior and posterior
355 amputations differed. The shape of the body at the cut site in anterior amputations was frequently
356 observed to be blunt, similar in shape to a specimen following wound healing (6 hpa) (Fig 2F), whereas
357 the tissue distal to the cut site in posterior amputations had a rounded tapered shape (Fig 2E). The
358 tapered shape in posterior amputations is different from the shape of the wound site in aged-matched
359 individuals (Stage 9) fixed at 6 hpa (compare Fig 2D, E). Our observations demonstrate that larvae not
360 only survive removal of a third of their body, but they continue to develop with a similar time course to
361 uncut animals.

362 *3.4 Cell proliferation*

363 One key feature of regeneration is the birth of new cells in the region of the wound site. Larval
364 development is a dynamic growth process that also exhibits cell proliferation. Stage 6 and 7 larvae have
365 a characteristic pattern of EdU incorporation following a one hour exposure to EdU. Specifically, there
366 are numerous EdU+ cells distributed throughout the trunk, straddling the midline (Fig 3A, B). In contrast,
367 by Stage 9, EdU+ cells are not ordinarily observed, apart from a few cells in the midgut or hindgut and
368 posterior growth zone (PGZ) (Fig 3C, 3D). To delineate between growth and a response to amputation,
369 we compared age-matched, uncut larvae with amputated larvae.

370 Anterior amputations show EdU incorporation near the amputation site. The initial pattern of EdU
371 incorporation in anterior amputations (6 hpa) is similar to the pattern observed in age-matched, uncut
372 controls (Fig 3E, 3I). This pattern of EdU incorporation persists in 1 dpa animals and in age matched
373 controls (Fig 3B, F, J). However, by 3 dpa, EdU+ cells are localized near the wound site in the anterior
374 ectoderm and occasionally in the mesoderm of the amputated animals (Fig 3G). EdU+ cells near the
375 wound site persist through 5 dpa in anterior ectoderm and mesoderm (Fig 3H). In contrast, there is a
376 notable lack of EdU+ cells in the corresponding body region of unamputated animals (Fig 3C, 3D). The
377 ratio of EdU+ cells to nuclei is higher in amputated animals at both 3 dpa and 5 dpa at the respective
378 amputation sites compared with the equivalent body region in uncut controls (Table 1). There is a
379 significant difference between the number of EdU+ cells in the anterior body region anteriorly
380 amputated larvae at 3 dpa and 5 dpa when compared to age-matched, uncut controls (One-way ANOVA
381 test) (Fig 3M).

382 Posterior amputations also show EdU incorporation localized near the wound site. In both cut and
383 uncut larvae, the number of EdU+ cells decrease over time in the anterior and middle sections of the
384 animal. While the initial pattern of EdU incorporation in cells at 6 hpa appears similar to that observed in
385 Stage 6 uncut controls (Fig 3I), there is a progressive shift toward expression localized to the cut site in
386 amputated larvae. Animals at 1 dpa have fewer EdU+ cells in the anterior 2/3 of the body (Fig 3J) in
387 comparison with uncut Stage 7 controls. By 3 dpa, EdU incorporation is not detected through the

388 anterior 2/3 of the body, and EdU+ cells are restricted to the area surrounding the cut site (Fig 3K). This
389 localized pattern of EdU incorporation persists through 5 dpa (Fig 3L). Furthermore, cut larvae have
390 more EdU+ cells in the posterior region than the uncut controls (Table 2). The number of EdU+ cells in
391 posterior sections of 3 dpa and 5 dpa larvae is significantly higher compared to age matched, uncut
392 controls (One-way ANOVA test) (Fig 3N). Additionally, there is a higher ratio of EdU+ cells/nuclei
393 localized to the wound site in posterior amputated larvae relative to anterior amputations. Together,
394 these data show a marked increase in cell proliferation at the wound site following both anterior and
395 posterior amputations.

396 *3.4 Expression of the stem cell marker vasa*

397 To further characterize the larval response to amputation, expression of the stem cell marker *vasa*
398 was analyzed by *in situ* hybridization (Dannenberg & Seaver, 2018; Juliano et al., 2010). In uncut larvae,
399 *vasa* expression is dynamic from Stage 6 through Stage 9 (Dill & Seaver, 2008). In Stage 6 larvae, there is
400 expression in the foregut, the mesoderm of the trunk and the PGZ (Fig 4A). By Stage 8, expression is
401 restricted to the foregut, the multipotent progenitor cell cluster (MPC), and the PGZ (Fig 4B). This
402 pattern continues through Stage 9 (with some variability in detection of the MPC) (Fig 4C).

403 *Vasa* expression is detected at the wound site in both anterior and posterior amputations. Initially,
404 the *vasa* expression pattern in both amputation groups is very similar to the observed pattern in uncut
405 controls (6 hr post amputation) (Fig 4D). However, by 2 dpa, there is *de novo* expression in the anterior
406 ectoderm at the amputation site of anteriorly cut larvae (Fig 4E). By 5 dpa, expression at the wound site
407 is no longer detected, although expression in the MPC and PGZ persists (Fig 4F). In posterior
408 amputations at 2 hpa, trunk mesodermal expression is continuous from one side of the animal to the
409 other and wraps around the posterior end of the body (Fig 4G). We interpret this expression along the
410 posterior face of the animal to be the result of wound healing that pulls the two lateral trunk domains of
411 expression together. At 2 dpa, *vasa* is expressed in the posterior mesoderm and ectoderm near the
412 wound site (Fig 4H). This expression near the wound site is also detectable 3 dpa (Fig 4I) and 4 dpa (data
413 not shown). In summary, *vasa* expression is detected at the wound site 2–3 dpa for both anterior and
414 posterior amputations.

415 *3.5 Generation of new tissue*

416 The presence of localized cell proliferation at the wound site (Fig 3G, 3H, 3K, and 3L) and what
417 appears to be growth of new tissue (Fig 2E) warranted a more detailed investigation of the tissue
418 surrounding the wound site. To distinguish between pre-exiting tissue and new tissue, the location of
419 the cut site was determined using the nervous system and musculature markers. We used a framework
420 commonly used for identifying the cut site in juvenile worms with an anti-acetylated tubulin antibody
421 marking the nervous system (Fig 1B). An abrupt change in the thickness of the connective nerves was
422 used to indicate the position of the cute site (Fig 1D, 5B, 5B', and 5C). An abrupt decrease in the density
423 of muscle fibers also indicated the location of the cut site (Fig 1E, Fig 5F and 5F'). Typically, there was a
424 precise concordance in position between an abrupt change in muscle fiber density and thickness of
425 connective nerves. Therefore, we could consistently identify the location of the cut site using these two
426 markers.

427 The identification of the cut site in amputated larvae allowed us to identify new tissue and
428 quantify tissue distal to the amputation site. No evidence of significant growth of tissue was detected in

429 anterior amputations between 6 hpa and 3 dpa (see Table 3). In contrast, there was significant growth in
430 posterior amputations between 6 hpa and 5 dpa. Additional measurements of posterior amputations
431 indicated a significant change in body width (body width at the mouth compared to immediately
432 posterior to the cut site) between 6 hpa and 5 dpa. This information is consistent with the presence of
433 new growth in posterior amputations; regenerated tissue is often more narrow than the width of the
434 original tissue. While the position of the cut site indicated by muscle and nerves indicated new growth,
435 there was one measurement that did not. Measurements from the posterior end of the pigmented gut
436 to the posterior of the animal for both the 6 hpa stage 9 and 5 dpa larvae did not show a significant
437 difference between these two groups.

438 We next characterized the nervous system and musculature of the tissue distal to the cut site.
439 Similar to what was observed in 6 hpa control larvae (Fig 5D), anterior amputations in 3 dpa larvae
440 lacked clear evidence of neurites and muscle fibers distal to the wound site (Fig 5 E–E”). In posteriorly
441 amputated larvae, a mixture of results was observed. In 2 dpa posteriorly amputated larvae with a
442 discernable cut site and new growth, neuronal projections distal to the amputation site were observed
443 that were not detected in 6 hpa larvae (Fig 5B, 5F, 5F’, 5F’’). There were also cases in which there was
444 seemingly no change in the larval nervous system (Fig 5G; n = 165/395). Cases in which new growth was
445 not observed lend confidence to those instances when we observed processes distal to the cut site
446 (compare Fig 5F’’ and 5G). At 5 dpa, nerve processes persisted in tissue distal to the cut site (Fig 5H,
447 5H’). These longitudinal nerve processes are located at the midline and span the length of the new
448 tissue. Additionally, there were circumferential processes similar to the orientation of peripheral nerves,
449 although these processes were somewhat disorganized relative to peripheral nerves in uncut animals
450 (Fig 5H’). These neuronal processes are oriented medial to lateral, extending from the midline. The
451 entire region of the new tissue has a lower density of muscle fibers relative to the preexisting tissue (Fig
452 5B, 5H’). The muscle fibers that are present are predominately longitudinal muscle fibers. In many cases,
453 individual longitudinal muscle fibers appear to extend from preexisting tissue into tissue distal to the
454 amputation site (Fig 5H”, arrow), whereas circular muscle fibers were only occasionally observed
455 posterior to the amputation site. These circular fibers are unlikely associated with a telotroch because
456 amputated larvae lack evidence of regrown ciliary bands. A similar arrangement of muscle and nerve
457 fibers in the tissue distal to the amputation site is present in animals 7 dpa (data not shown). While we
458 observed multiple tissue types distal to the cut site, we did not observe evidence of new segmentation.
459 Conventionally, newly formed segments are characterized by the appearance of new ganglia, regularly
460 spaced circumferential peripheral nerves and segmental boundaries. The nervous system distal to the
461 cut site did not organize into ganglia by 7 dpa, and peripheral nerves were disorganized. We did not
462 observe segmental boundaries in the ectoderm. In conclusion, new tissue growth was observed along
463 with changes in organization of the nervous system and musculature in posteriorly amputated larvae,
464 although there was a lack of new tissue in anteriorly amputated larvae.

465 *3.6 Neural specification and differentiation*

466 Next, we sought to determine if the neural and muscle cell types observed distal to the amputation
467 site resulted from the birth of new cells. We rationalized that expression of molecular markers of cell
468 fate specification and differentiation in the tissue distal to the amputation site indicated birth of new
469 cells. For the nervous system, gene expression patterns of neural specification (*ash1*) and neural
470 differentiation markers (*elav*) were analyzed near the wound site (Meyer & Seaver, 2009). In *C. teleta*,
471 *ash1* is a marker of neural specification during initial neurogenesis of the brain and VNC (Meyer &

472 Seaver, 2009; Sur et al., 2017). In Stage 6 larvae, *ash1* is expressed in the brain, foregut, ventral neural
473 ectoderm, PGZ, and the mesoderm in the pygidium (Fig 6A). By Stage 9, *ash1* expression is restricted to
474 the foregut and PGZ (Fig 6B). In anterior amputations, the pattern observed at 6 hpa for *ash1* expression
475 mirrors that of uncut Stage 6 larvae, with the notable exception of missing brain expression due to the
476 removal of the head (Fig 6C). In 3 dpa specimens, *ash1* is expressed in both the anterior ectoderm and
477 pharynx (Fig 6D). Expression in the ectoderm can be regarded as *de novo ash1* anterior expression since
478 age-matched, uncut controls lack anterior ectoderm expression (compare panels Fig 6B and 6D, E) (n
479 =32/39). The novel anterior ectodermal expression of *ash1* at 3 dpa was present in a punctate pattern
480 similar to the pattern observed in the anterior ectoderm during *C. teleta* brain development. In contrast,
481 expression in the pharynx corresponds with expression in age matched uncut controls, albeit with fewer
482 cells.

483 After observing novel anterior neural specification following amputation, the next step of
484 neurogenesis was analyzed by characterizing the expression pattern of *elav*, a marker of differentiating
485 neurons. Between Stages 6 and 9 in uncut controls, *elav* is expressed in the brain and the VNC (Fig 6F &
486 G). In 6 hpa anterior amputations, *elav* is expressed only in the VNC (Fig 6H). This expression pattern
487 persists through 3 dpa, with no new expression domains observed in amputated animals (n =21/22) (Fig
488 6I). In the one differing case of the 22 scored animals, there were a few *elav*-expressing cells in the
489 anterior ectodermanteriorly located cells. These cells are part of the pharynx that abnormally everted
490 during morphogenesis.

491 *3.7 Amputation induces expansion of MyoD expression*

492 We also examined the expression of *MyoD*, a gene known for its role in muscle specification and
493 differentiation (Zammit, 2017). In uncut larvae, *MyoD* is expressed in the mesoderm of the posterior
494 trunk segments at Stage 6 (Fig 7A) and Stage 9 (Fig 7B). There is a developmental progression from
495 anterior to posterior in the larval trunk, with the more mature segments having an anterior position
496 (Seaver et al., 2005). Thus, *MyoD* is expressed in the younger and newly forming segments. Six hours
497 after both anterior and posterior amputations (6 hpa), expression is restricted to the posterior portion
498 of the trunk (Fig 7 C & E), similar to what is observed in uncut controls. At 7 dpa in anterior amputees
499 (Fig 7D) and at 3 dpa in posterior amputees (Fig 7F), there is a drastic expansion of *MyoD* mesodermal
500 expression along the entire length of the trunk. This expansion in *MyoD* expression is in pre-existing
501 tissue in older segments and includes tissue distant from the wound site in the case of posterior
502 amputations.

503 *3.8 Rare regeneration of differentiated cell types*

504 Following amputations, a few differentiated cell types occasionally regenerated, namely the
505 larval eyes and cilia. Larvae have two cerebral eyes, with each eye consisting of three cells: a pigment
506 cell (Fig 8A), a sensory cell (Fig 8C), and a support cell (Yamaguchi & Seaver, 2013). The pigment cell is
507 readily visible by its orange pigment granules and the sensory cell can be visualized by immunolabeling
508 with the antibody 22C10 (Yamaguchi & Seaver, 2013). Currently, we are unable to assess the presence
509 of the support cell. In uncut Stage 9 larvae, the pigment cells are located slightly anterior, if not inline,
510 with the prototroch, in a lateral position (Fig 8A). The sensory cell in uncut Stage 9 larvae (Fig 8C) is
511 located immediately adjacent and lateral to the pigment cell and has an axonal projection extending
512 from the cell body to the external surface of the ectodermal epithelium. The pigment and sensory cells
513 were scored as independent characters. Following head amputation, a few pigment cells regenerated,

514 and they are variable in location and number (n = 28/420; 3-5 dpa). Additionally, the pigment cells in
515 amputated larvae are ectopically positioned. For example, as seen in Fig 8B, there is a pigment cell in
516 proximity to the midgut. Regenerated sensory cells were also observed in amputated larvae and also
517 exhibited variability in location (n= 8/220, 3 –7 dpa). Axon projections in regenerated sensory cells
518 extended to the outer ectodermal surface of the animals (Fig 8D). There was a higher percentage of
519 cases with regenerated pigment cells (7%) compared with sensory cells (4%) in anterior amputations (Fig
520 8G). Summation of the total number of pigment cells and sensory cells indicates that at least one cell of
521 the eye regenerated in 6% of cases amputated (n = 36/640).

522 We were surprised by the appearance of new larval eye cells in amputated *C. teleta* larvae since
523 regeneration of anterior structures is not reported in adults (Yamaguchi & Seaver, 2013). Therefore, we
524 conducted a similar experiment with juveniles. Four-week-old juveniles were amputated immediately
525 anterior to the mouth, removing the eye cells. After screening for successful wound healing and visual
526 inspection that pigment cells were removed, a subset of the amputated juveniles was fixed at 4 hpa to
527 confirm the removal of the sensory cells (n =21/21). No pigment cells were observed in amputated
528 juveniles at 7 dpa (n = 0/43). However, a small proportion of cases with eye sensory cells were observed
529 (Fig 8E) (n = 6/43; 14%). Regenerated sensory cells were ectopically located (compare Fig 8E and 8F).
530 Five of the six juveniles with regenerated sensory cells had a small portion of brain present in the
531 anterior of the animal; only one case lacking a brain had a sensory cell. In summary, pigment cells did
532 not regenerate in juveniles, although sensory cells were detected in a small fraction of cases. These rare
533 instances of eye sensory cell regeneration represented the most dramatic phenotype observed following
534 juvenile anterior amputations.

535 There are four external ciliated structures in *C. teleta* larvae: prototroch, neurotroch, telotroch,
536 and pygidial cilia (Fig 9A, B). The prototroch and telotroch are composed of relatively long cilia
537 (prototroch cilia length ~25-30 microns and telotroch cilia length ~20-28 microns), and the neurotroch
538 and pygidium have short cilia (neurotroch cilia length ~ 8-10 microns, pygidium length ~5-7 microns). At
539 6 hpa, larvae lacked long cilia at the cut site (Fig 9 C and 9D), due to amputation of the prototroch and
540 telotroch in anterior and posterior amputations, respectively. At 5 dpa, short cilia (approximately 8
541 microns in length) were observed in rare cases (n = 12/161; 7%) at the anterior end of anteriorly cut
542 animals, distal to the amputation site (compare Fig 9E and F). Long cilia were not observed following
543 anterior amputations (n = 0/161). While rare (n = 22/370; 6%), both long (~25 microns) and short (~9
544 microns) cilia appeared distal to the cut site 3–7 days after posterior amputations (compare Fig 9G with
545 9H and 9H').

546 *3.9 Metamorphosis following amputation*

547 *C. teleta* is competent and can be induced to undergo metamorphosis into juveniles as Stage 9
548 larvae (Burns et al., 2014). Following amputation, larvae were screened for stereotypical signs of
549 successful settlement and metamorphosis following the definition of Cohen and Pechenik (1999). These
550 changes include a loss of swimming and initiation of burrowing behavior, loss of both ciliary bands
551 (telotroch and prototroch), and the appearance of an elongated, worm-like body shape. Uncut,
552 uninduced control larvae swam with their prototroch and telotroch bands intact for the duration of the
553 experiment (Fig 10A) (2 hr, n = 532/534). In contrast, virtually all larvae in the induced, unamputated
554 control group successfully underwent metamorphosis within two hours of exposure to the metamorphic
555 cue, settling on the bottom of the dish, dropping their cilia, adopting burrowing behavior, and extending

556 in length along the anterior-posterior axis (Fig 10B) (n = 203/207). Both sets of amputated larvae
557 followed a similar pattern to what was observed for unamputated larvae. Specifically, one day after
558 anterior amputation, larvae either continued to swim in the water column in the absence of a
559 metamorphic cue (Fig. 10C) (n=65/66) or settled to the bottom of the dish and underwent
560 metamorphosis within two hours of exposure to a metamorphic cue (Fig. 10D) (n=135/136). Similarly,
561 individuals whose posterior ends had been removed retained their prototrochal bands and continued to
562 swim in the absence of a metamorphic cue (Fig. 10E, arrow) (n=65/65), yet underwent rapid settlement
563 and metamorphosis within two hours of exposure (Fig. 10F) (n=143/144). In the absence of an induction
564 cue, amputated larvae continued to swim in the water column and retained their ciliary bands for
565 several days, demonstrating that amputation itself does not induce metamorphosis (Fig 9E and 9F).
566 Together, these results demonstrate *C. teleta* larvae can detect a metamorphic cue and successfully
567 execute metamorphosis in the absence of either anterior or posterior structures.

568 **4. Discussion**

569 *4.1 Limited regeneration in C. teleta larvae*

570 This study demonstrates that the initial events in response to amputation appear to be quite
571 similar between *C. teleta* larvae and juveniles. Following both anterior and posterior amputation, larvae
572 wound heal in a similar time frame as previously reported for posterior amputation of juveniles (i.e.,
573 within 6 hpa) (de Jong & Seaver, 2016). Following wound healing, EdU+ cells appear localized at the
574 wound site at 2 dpa in juvenile posterior regeneration, and the number of EdU+ cells increase over time
575 (de Jong & Seaver, 2016). EdU incorporation in anterior-facing wound sites in juveniles of *C. teleta* has
576 not been formally characterized. In both anterior and posterior larval amputations, EdU is incorporated
577 near the wound site by 3 dpa and this persists through 5 dpa, comparable to the pattern of EdU
578 incorporation at the wound site in regenerating juveniles. There is a difference in the number of EdU+
579 cells between anterior and posterior amputations in larvae, with posterior amputations exhibiting more
580 EdU+ cells. One difference in cell proliferation patterns between juveniles and larvae is a change in
581 position of the localized EdU+ cells. During posterior regeneration in juveniles, localization of EdU+ cells
582 progressively shifts anteriorly to a subterminal position, a shift that corresponds with the re-
583 establishment of the juvenile PGZ. We did not observe such a shift in larvae. It is interesting to note that
584 in adults of the annelid *Paranais litoralis*, BrdU is incorporated near the anterior wound site even though
585 these animals have lost the ability to regenerate their heads (Bely & Sikes, 2010). This finding, along with
586 our results in *C. teleta* larvae, emphasize that a block in regeneration can occur subsequent to the
587 initiation of cell division at the wound site, and cell division at the wound site is not a reliable predictor
588 of successful regeneration.

589 Interestingly, expression of the stem cell marker *vasa* at the wound site was observed in both
590 anteriorly and posteriorly amputated larvae. In successful posteriorly regenerating juveniles, *vasa* is
591 expressed locally at the wound site at 2 dpa and persists for several days (de Jong & Seaver, 2017). In
592 larvae, the duration of *vasa* expression and proportion of cases is different between anterior and
593 posterior amputations. In anterior amputations, *vasa* is expressed in the anterior ectoderm in
594 approximately 1/3 of cases and is transient, detectable at 2 dpa but not 5 dpa. Conversely, localized *vasa*
595 expression is observed at 2 dpa and persists through 5 dpa in posterior amputations. We interpret the
596 localized expression of *vasa* at the posterior wound site as either the result of *de novo* expression or
597 expression maintained from an earlier stage (i.e., 6 hpa). The spatial and temporal patterns of EdU

598 incorporation and *vasa* expression are very similar in posterior amputations. In contrast, *vasa* expression
599 has a shorter duration than EdU incorporation near the wound site in anterior amputations. We
600 hypothesize that these differences between anterior and posterior amputations is related to the new
601 tissue growth in posterior amputations that is absent following anterior amputations.

602 Additional features of juvenile posterior regeneration are the presence of neural projections
603 into the wound site and muscle reorganization distal to the amputation site. In juveniles, this
604 phenomenon is observed approximately at 2 dpa (de Jong & Seaver, 2016). In larval posterior
605 amputations, neurites are present distal to the cut site by 2 dpa. However, these neurites were not
606 observed in larval anterior amputations. With respect to muscle fiber organization, there is an abrupt
607 transition between the presence and absence of muscle fibers distal to the cut site in both juveniles and
608 larval posterior amputations that was not observed in larval anterior amputations. We were unable to
609 determine whether fibers present distal to the amputation site in posterior larval amputations resulted
610 from birth of new neural or muscle cells or from the extension of pre-existing cells.

611 To better understand the characteristics and development of the tissue distal to the cut site in
612 larvae, we characterized the specification and differentiation of cell types (i.e., neural cell types and
613 cilia) in amputated larvae. The timing of neural specification or differentiation in juveniles has not been
614 investigated in detail, but differentiated tissues are present by 7 dpa (de Jong & Seaver, 2016). Analysis
615 of *de novo ash1* expression indicates the specification of neural fates in larval anterior amputations.
616 Surprisingly, subsequent differentiation of neural tissues was not detectable, as illustrated by the
617 absence of *elav* expression in larval amputations. Anterior amputation of larvae results in incomplete
618 tissue and structure regeneration—an observation consistent with the response in juveniles to anterior
619 amputations. Despite a general lack of anterior structural differentiation in amputated larvae, we
620 surprisingly observed rare cases in which differentiated eye cells and cilia reappeared within 3–7 dpa.
621 Additionally, sensory eye cells (but not pigment cells) regenerated in juveniles at a higher proportion
622 than in larvae (14% in juveniles, 4% in larvae). While rare, the absence of eyes immediately following
623 amputation and the ectopic location of the observed eye cells made us confident that these cells are
624 regenerated eye cells in amputated larvae and juveniles. One possible explanation for the variation in
625 cilia and eye cell regeneration across individuals is variance in maternal nutritional output.

626 In summary, the beginning stages of regeneration (i.e., wound healing, localized cellular
627 proliferation, and expression of stem cell markers, etc.) occur in amputated larvae but there is a lack
628 complete replacement of lost tissue or of cell or tissue differentiation. These data indicate that *C. teleta*
629 larvae exhibit limited regeneration abilities relative to the successful posterior regeneration observed in
630 juvenile and adult stages. Additionally, detection of initial stages of regeneration in larvae suggests that
631 *C. teleta* has a gradual transition in regenerative potential, rather than a stark change in potential that
632 corresponds with the metamorphoric transition.

633 *4.2 Amputation-induced expression in preexisting tissue*

634 *MyoD* functions in muscle development and its expression in muscle progenitor cells is an indication
635 of myogenesis (Zammit, 2017; Rawls & Olson, 1997). In response to amputation, *MyoD* expression
636 expands across the length of the larval body in *C. teleta*, far from the wound site. This expanded
637 expression may result in an increase in muscle cell number to compensate for a decrease in body length
638 following amputation, although we did not observe an obvious increase in the number of muscle fibers 3
639 – 5 dpa. Alternatively, expanded expression of *MyoD* may be an injury-specific response that leads to

640 cell dedifferentiation and return to a precursor state. Such a precursor cell population may contribute to
641 regenerating tissue. It is notable that the induction of expanded *MyoD* expression occurs in the absence
642 of a complete regeneration response. Regardless, future functional work is needed to better understand
643 the implications of this change in *MyoD* expression in response to amputation. Changes in gene
644 expression in response to amputation has previously been documented in *C. teleta* and other annelids
645 (de Jong & Seaver, 2016; Kozin et al., 2017; Pfeifer et al., 2012; Takeo et al., 2008). However, most
646 examples documented to date are changes in expression of positional identity genes, and their new
647 expression likely reflects repatterning of the body fragment in response to amputation.

648 *4.3 Metamorphosis following amputation*

649 Amputated *C. teleta* larvae undergo successful metamorphosis. We were surprised to observe
650 metamorphosis following anterior amputations. In other spiralians, it has been hypothesized that the
651 brain and other anterior sensory organs function in the detection and response to metamorphic cues
652 (Chartier et al., 2018; Conzelmann et al., 2013; Hadfield, 2010; Hadfield et al., 2000). In *C. teleta*, chemo-
653 sensitive ciliated cells in the head ectoderm were proposed to relay metamorphosis signals directly to
654 the cerebral ganglia (Biggers & Laufer, 1999). More recently, a study hypothesized that the inductive
655 signal for metamorphosis is detected by sensory neurons that innervate the dorsal pharyngeal pad of
656 the pharynx (Biggers et al., 2012). If the metamorphic cue was detected by anterior neurons, we would
657 expect that removing the head would prevent metamorphosis. However, our results demonstrate that
658 the brain is not required for detecting the metamorphic cue or for undergoing metamorphosis in *C.*
659 *teleta*, supporting the hypothesis that detection of metamorphic cues in *C. teleta* likely occur in the
660 pharynx. It was similarly demonstrated in the polychaete *Hydroides elegans* that apical sensory neurons
661 are not necessary for successful metamorphosis (Nedved et al., 2021), suggesting that the brain may not
662 be necessary for metamorphosis in some annelids.

663 It is yet to be determined whether the amputations performed during larval stages have lasting
664 effects on survival and growth following metamorphosis. In addition, it remains to be seen whether
665 juveniles induced from posteriorly amputated larvae redevelop posterior growth zones, can generate
666 additional segments, or are capable of posterior regeneration. Future studies could examine the
667 regeneration potential of juveniles that result from posteriorly amputated larvae. Additionally, it could
668 be interesting to determine if juveniles induced from anterior amputated larvae are capable of posterior
669 regeneration in the absence of a brain.

670 *4.4 Larval regeneration in marine invertebrates*

671 The regenerative potential of an animal can vary significantly across its life stages. In the literature,
672 larvae with reduced regenerative ability relative to adults are described as having "attempted" or
673 "limited" regeneration (Vickery et al., 2001). Using this convention, we categorize *C. teleta* larvae as
674 having limited regeneration. Here, we show that *C. teleta* gains regeneration ability over its life cycle and
675 exhibits different regeneration abilities between larval and juvenile stages. To our knowledge, published
676 studies characterizing larval regeneration abilities in other annelid larvae are scarce.

677 Other bilaterian taxa suffer from a similar dearth in sampling larval and immature stages for their
678 regenerative abilities. Within Spiralia, larval regeneration has been examined in one nemertean species.
679 Similar to annelids, nemertean adult regeneration is variable (Zattara et al., 2019; Zattara & Fernández-
680 Alvarez, 2022). *Maculaura alaskensis* appears to have high regenerative potential as early stage larvae

that progressively decreases with maturation until it stabilizes as an adult capable of posterior regeneration (Hiebert & Maslakova, 2015). Younger *M. alaskensis* larvae are five times more likely to regenerate than older larvae following amputation (Moss, 2017). In Ecdoysozoa, the other protostome clade, regeneration ability is generally restricted to appendages, rather than along the main body axis (Brenneis et al., 2023). However, recent work shows that immature instars of the sea spider *Pycnogonum littorale* can regenerate the midgut and gonads as well as appendages following bisection. Adult counterparts of *P. littorale* cannot regenerate and do not even survive the amputations, suggesting that regeneration ability is restricted to the immature instar stages (Brenneis et al., 2023).

Deuterostome larvae have been better surveyed for regeneration ability and there are numerous documented examples. The hemichordate *Ptychodera flava* has the ability to repeatedly regenerate all body parts when cut transversely or decapitated as an adult (Humphreys et al., 2022). Although *P. flava* larvae can regenerate along its main body axis, it does not regenerate as well as the adults. In addition, regeneration ability differs across the larval body. Specifically, ventral regions of *P. flava* larvae regenerate better than dorsal regions and posterior segments regenerate better than anterior segments (Luttrell et al., 2018). The larval tail of the cephalochordate *Branchistoma floridae* regenerates multiple tissues faster than adults following similar amputations (Zou et al., 2021). Unlike other clades, echinoderm larvae have been widely surveyed for regenerative potential in all classes with documented adult whole body regeneration abilities (Cary et al., 2019; Vickery et al., 2001). Asteroids and echinoid larvae, such as *Patiria miniate,* can regenerate completely, regardless of developmental stage, demonstrating a stable regenerative ability throughout life (Oulhen, 2016; Carnevali, 2006; Vickery et al., 2002). In crinoids, there appears a trend of increasing regenerative potential over developmental time. For example, crinoid larvae display limited ability to regenerate body parts, with early-stage *Antedon rosacea* larvae regenerate more poorly than late-stage larvae (Carnevali, 2006). In contrast, adults can replace lost structures even when reduced to 1/5 of the original body size (Carnevali, 2006). In summary, no clear trends of increasing or decreasing regeneration abilities across the life cycle emerge from regeneration studies either within or across taxa, suggesting changes in regeneration ability across the life cycle is a variable trait.

Although we cannot currently identify trends reflecting how regeneration abilities change between larval and adult stages from a phylogenetic perspective, we can consider the impact of life history factors. Factors such as feeding (de Jong & Seaver, 2016; Özpolat et al., 2016; Zattara & Bely, 2013), duration of larval stage, and sublethal predation (Schoeman and Simon, 2023; Stewart, 1996) may better correlate with the regenerative abilities observed in an individual species. Unlike *C. teleta*, *M. alaskensis*, *P. flava*, and *P. miniate* larvae feed and display an ability to replace complex structures following amputation. *M. alaskensis* and *P. miniate* can swim in the water column for weeks or months (Moss, 2017; Cary et al., 2019) and *P. flava* for up to 300 days (Luttrell et al., 2018). In contrast, larvae of *C. teleta* and the crinoid *A. rosacea* are non-feeding (Vickery et al., 2001) and have a short larval period before undergoing metamorphosis. *C. teleta* larvae swim in the water column for hours to a few days, and some crinoids for up to 10 days before settlement (Nakano et al., 2003). It has been previously proposed that the longer an animal is in the water column and vulnerable to predation, the greater risk there is of sublethal injury (Vickery & McClintock, 1998). Sublethal damage could act as an evolutionary pressure to select for a robust regenerative ability. To that end, there may not be a strong selective advantage for regeneration in non-feeding, short lived, brood dwelling larvae like *C. teleta*.

4.5 Future directions

This study demonstrates differences in regenerative ability across developmental stages of *Capitella teleta*. Future studies could investigate physiological, cellular, and molecular differences between larvae and juveniles in response to amputation. One such difference may relate to nutritional status. It has been demonstrated that the extent of regeneration in *C. teleta* juveniles and other annelids can fluctuate depending on nutrition intake (de Jong & Seaver, 2016; Zattara & Bely, 2013). Because *C. teleta* larvae are non-feeding, limited energy resources may contribute to their regeneration limitations. This nutrition hypothesis could be tested by two separate approaches. In the first, cells with high yolk content can be deleted in early-stage embryos to reduce maternally contributed nutrition. Previous work demonstrated that such deletions result in morphologically normal, albeit smaller larvae (Pernet et al., 2012). These larvae would have a reduced nutritional supply and may exhibit a further reduction in regenerative potential to what was observed in this study. The second approach would involve investigating regeneration abilities in a different annelid with a feeding larval form. A feeding larva with more nutritional resources may exhibit full regenerative abilities following amputation. Additionally, an annelid with a longer larval period would have more time to completely regenerate lost tissue following amputation during the early larval period, while also continually feeding.

The timing of cell maturation may also limit larval regeneration and explain differences between larval and juvenile regenerative abilities in *C. teleta*. An example of one such developmental constraint may be in the timing of stem cell maturation. A previous study proposed that stem cells travel from the multipotent progenitor cell (MPC) cluster to the wound site during juvenile regeneration (de Jong & Seaver, 2017). MPC cells in larvae may be immature, thereby preventing these stem cells from positively contributing to successful regeneration. Specifically, nascent stem cells may not be capable of self-renewal or migration, or of contributing to the blastema (Juliano et al., 2010). The number of cells in the MPC cluster does not increase during larval development (de Jong & Seaver, 2017), suggesting these cells may be quiescent during this time. A heterotopic transplant of a mature MPC cluster from juveniles into larvae would test this hypothesis, and an increased regenerative ability in larvae following transplantation would be expected. Such experiments in *C. teleta* regeneration might lead to a better understanding of the role that development has on regeneration.

Future studies can characterize the regeneration ability of other annelid larvae, particularly those whose adults have different regenerative potential than that of *C. teleta*. A correlation between adult and larval regenerative potential within individual species may exist. For example, there may be anterior regenerative ability in larvae in a species capable of anterior regeneration as an adult. If this correlation holds, the larvae of *Chaetopterous pergamentaceus* (Cuvier & Latreille, 1829) (formally *variopedatus*) would be predicted to regenerate both anterior and posterior structures. Adult *C. pergamentaceus* can regenerate anteriorly following amputations at segment 15 or more anterior and can regenerate posteriorly following amputation at any segment (Berrill, 1928; Cuvier & Latreille, 1829). Extensive additional sampling is needed before we can meaningfully determine whether the pattern observed in *C. teleta* is representative of other annelids. Additional sampling across annelids will also provide insight as to the extent of variation in larval regeneration abilities, and whether larval regenerative ability is as common as adult regenerative ability.

Acknowledgements

We thank Brent Foster, Lauren Kunselman, and Katie Feerst for critical reading of the manuscript.

766 **Author Contributions**

767 Conceived and designed the experiments: AAB ECS. Performed the experiments: AAB. Analyzed the
768 data: AAB ECS. Contributed reagents/materials/analysis tools: ECS AAB. Wrote the paper: AAB ECS.

769

References

Alvarado, A. S. (2000). Regeneration in the metazoans: why does it happen? *BioEssays*. https://doi.org/10.1002/(SICI)1521-1878(200006)22:6

Bely, A. E. (2006). Distribution of segment regeneration ability in the *Annelida*. *Integrative and Comparative Biology*, *46*(4), 508–518. https://doi.org/10.1093/icb/icj051

Bely, A. E., & Sikes, J. M. (2010). Latent regeneration abilities persist following recent evolutionary loss in asexual annelids. *Proceedings of the National Academy of Sciences of the United States of America*, *107*(4), 1464–1469. https://doi.org/10.1073/pnas.0907931107

Berrill, N.J. (1928). Regeneration in the polychaet *Chaetopterus variopedatus*. *Journal of Marine Biological Association of the United Kingdom*, 15(1), 151-158. https://doi.org/10.1017/S0025315400055594

Biggers, W. J., & Laufer, H. (1999). Settlement and metamorphosis of *Capitella* larvae induced by juvenile hormone-active compounds is mediated by protein kinase C and ion channels. 196(2), 187–198. https://doi.org/10.2307/1542564

Biggers, W. J., Pires, A., Pechenik, J. A., Johns, E., Patel, P., Polson, T., & Polson, J. (2012). Inhibitors of nitric oxide synthase induce larval settlement and metamorphosis of the polychaete annelid *Capitella teleta*. *Invertebrate Reproduction and Development,* 56(1), 1–13. https://doi.org/10.1080/07924259.2011.588006

Blake, J.A., Grassle, J.P., & Eckelbarger, K.J. (2009). *Capitella teleta*, a new species designation for the opportunistic and experimental *Capitella* sp. I, with a review of the literature for confirmed records. *Zoosymposia*, 2(1), 25– 53. DOI:10.11646/zoosymposia.2.1.6

Boyle, M. J., & Seaver, E. C. (2008). Developmental expression of *foxA* and *gata* genes during gut formation in the polychaete annelid, *Capitella* sp. I. *Evolution & Development*, 10(1), 89–105. https://doi.org/10.1111/J.1525-142X.2007.00216.X

Brenneis, G., Frankowski, K., MaaB, L., & Scholtz, G. (2023) The sea spider *Pycnogonum littorale* overturns the paradigm of the absence of axial regeneration in molting animals. *PNAS*, 120(5). https://doi.org/10.1073/pnas.221727120

Brockes, J. P. (1997). Amphibian limb regeneration: rebuilding a complex structure. *Science*, 276(5309), 81–87. https://doi.org/10.1126/SCIENCE.276.5309.81

Burns, R. T., Pechenik, J. A., Biggers, W. J., Scavo, G., & Lehman, C. (2014). The B vitamins nicotinamide (B3) and riboflavin (B2) stimulate metamorphosis in larvae of the deposit-feeding polychaete capitella teleta: implications for a sensory ligand-gated ion channel. *PLoS ONE*, 9(11). https://doi.org/10.1371/journal.pone.0109535

Byrnes, E. F. (1904). Regeneration of the anterior limbs in the tadpoles of frogs. *Archiv Für Entwicklungsmechanik Der Organismen*, *18*(2), 171–177. https://doi.org/10.1007/BF02163652

Carnevali, C. (2006). Regeneration in echinoderms: repair, regrowth, cloning. *Invertebrate Survival Journal.* 3(1), 64-76.

Carnevali, M. D. C., Lucca, E., & Bonasoro, F. (1993). Mechanisms of arm regeneration in the feather star *Antedon mediterranea*: healing of wound and early stages of development. *Journal of Experimental*

Zoology, *267*(3), 299–317. https://doi.org/10.1002/JEZ.1402670308

Cary, G. A., Wolff, A., Zueva, O., Pattinato, J., & Hinman, V. F. (2019). Analysis of sea star larval regeneration reveals conserved processes of whole-body regeneration across the metazoa. *BMC Biology*, *17*(1), 16. https://doi.org/10.1186/s12915-019-0633-9

Chartier, T. F., Deschamps, J., Dürichen, W., Jékely, G., & Arendt, D. (2018). Whole-head recording of chemosensory activity in the marine annelid *Platynereis dumerilii*. *Open Biology*, *8*(10). https://doi.org/10.1098/RSOB.180139

Cohen, R. A., & Pechenik, J. A. (1999). Relationship between sediment organic content, metamorphosis, and postlarval performance in the deposit-feeding polychaete *Capitella* sp. I *Journal of Experimental Marine Biology and Ecology*, *240*, 1–18. https://doi.org/10.1016/S0022-0981(99)00047-7

Conzelmann, M., Williams, E. A., Tunaru, S., Randel, N., Shahidi, R., Asadulina, A., Berger, J., Offermanns, S., & Jékely, G. (2013). Conserved MIP receptor-ligand pair regulates *Platynereis* larval settlement. *Proceedings of the National Academy of Sciences of the United States of America*, *110*(20), 8224–8229. https://doi.org/10.1073/PNAS.1220285110/-/DCSUPPLEMENTAL

Cuvier, G., & Latreille, P. A. (1829). Le règne animal distribué d'après son organisation, pour servir de base à l'histoire naturelle des animaux et d'introduction à l'anatomie comparée. Chez Déterville. https://doi.org/10.5962/bhl.title.49223

Dannenberg, L. C., & Seaver, E. C. (2018). Regeneration of the germline in the annelid *Capitella teleta*. *Developmental Biology*, *440*(2), 74–87. https://doi.org/10.1016/j.ydbio.2018.05.004

de Jong, D. M., & Seaver, E. C. (2016). A stable thoracic hox code and epimorphosis characterize posterior regeneration in *Capitella teleta*. *PLOS ONE*, *11*(2), e0149724. https://doi.org/10.1371/journal.pone.0149724

de Jong, D. M., & Seaver, E. C. (2017). Investigation into the cellular origins of posterior regeneration in the annelid *Capitella teleta*. *Regeneration (Oxford, England)*, *5*(1), 61–77. https://doi.org/10.1002/reg2.94

del Olmo, I., Verdes, A., & Alvarez-Campos, P. (2022) Distinct patterns of gene expression during regeneration and asexual reproduction in the annelid *Pristina leidyi*. *Journal of experimental zoology*. doi: 10.1002/jez.b.23143

Dill, K. K., & Seaver, E. C. (2008). *Vasa* and *nanos* are coexpressed in somatic and germ line tissue from early embryonic cleavage stages through adulthood in the polychaete *Capitella* sp. I. *Development Genes and Evolution*, *218*(9), 453–463. https://doi.org/10.1007/s00427-008-0236-x

Giani, V. C., Yamaguchi, E., Boyle, M. J., & Seaver, E. C. (2011). Somatic and germline expression of *piwi* during development and regeneration in the marine polychaete annelid *Capitella teleta*. *EvoDevo*, *2*(1). https://doi.org/10.1186/2041-9139-2-10

c. Good Calculators. [online software]. https://goodcalculators.com/one-way-anova-calculator/

Grassle, J., & Grassle, J. F. (1976). Sibling species in the marine pollution indicator *Capitella* (polychaeta). *Science* 192(4239),567– 569. DOI: 10.1126/science.1257794

Hadfield, M. G. (2010). Biofilms and marine invertebrate larvae: What bacteria produce that larvae use

to choose settlement sites. *Annual review of marine science*, *3*, 453–470. https://doi.org/10.1146/ANNUREV-MARINE-120709-142753

Hadfield, M. G., Meleshkevitch, E. A., & Boudko, D. Y. (2000). The apical sensory organ of a gastropod veliger is a receptor for settlement cues. *Biological Bulletin*, 198(1):67-76. doi: 10.2307/1542804

Harrison, R. G. (1898). The growth and regeneration of the tail of the frog larva - Studied with the aid of Born's method of grafting. *Archiv Für Entwickelungsmechanik Der Organismen*, *7*(2–3), 430–485. https://doi.org/10.1007/BF02161494

Hiebert, T. C., & Maslakova, S. (2015). Integrative taxonomy of the *Micrura alaskensis* Coe, 1901 species complex (Nemertea: Heteronemertea), with descriptions of a new genus maculaura gen. nov. and four new species from the NE pacific. *Zoological Science*, *32*(6), 615–637. https://doi.org/10.2108/ZS150011

Humphreys, T., Weiser, K., Arimoto, A., Sasaki, A., Uenishi, G., Fujimoto, B., Kawashima, T., Taparra, K., Molnar, J., Satoh, N., Marikawa, Y., & Tagawa, K. (2022) Ancestral stem cell reprogramming genes active in hemichordate regeneration. *Frontiers in Ecology and Evolution*. doi:10.3389/fevo.2022.769433

Jeffery, W. R. (2015). Regeneration, stem cells, and aging in the tunicate *Ciona*: insights from the oral siphon. *International Review of Cell and Molecular Biology*, *319*, 255–282. https://doi.org/10.1016/bs.ircmb.2015.06.005

Juliano, C. E., Swartz, S. Z., & Wessel, G. M. (2010). A conserved germline multipotency program. *Development*, *137*(24), 4113–4126. https://doi.org/10.1242/DEV.047969

Kostyunchenko, R.P. (2022) *Nanos* is expressed in somatic and germline tissue during larval and post-larval development of the annelid *Alitta virens*. *Genes.*13, 270. http://doi.org/10.3390/genes13020270

Lowry, R. (2023) vassarstats [online software]. http://vassarstats.net/anova1u.html

Luttrell, S. M., Su, Y. H., & Swalla, B. J. (2018). Getting a head with *Ptychodera flava* larval regeneration. *Biological Bulletin*, *234*(3), 152–164. https://doi.org/10.1086/698510

Meyer, N. P., Boyle, M. J., Martindale, M. Q., & Seaver, E. C. (2010). A comprehensive fate map by intracellular injection of identified blastomeres in the marine polychaete *Capitella teleta*. *EvoDevo*, *1*(1). https://doi.org/10.1186/2041-9139-1-8

Meyer, N. P., Carrillo-Baltodano, A., Moore, R. E., & Seaver, E. C. (2015). Nervous system development in lecithotrophic larval and juvenile stages of the annelid *Capitella teleta*. *Frontiers in Zoology*, 12(1), 1–27. https://doi.org/10.1186/s12983-015-0108-y

Meyer, N. P., & Seaver, E. C. (2009). Neurogenesis in an annelid: Characterization of brain neural precursors in the polychaete *Capitella* sp. I. *Developmental Biology*, *335*(1), 237–252. https://doi.org/10.1016/J.YDBIO.2009.06.017

Nakano, H., Hibino, T., Oji, T., Hara, Y., & Amemiya, S. (2003) Larval stages of a living sea lily (stalked crinoid echinoderm). Nature 421, 158–160. https://doi.org/10.1038/nature01236

Nedved, B. T., Freckelton, M. L., & Hadfield, M. G. (2021). Laser ablation of the apical sensory organ of *Hydroides elegans* (Polychaeta) does not inhibit detection of metamorphic cues. *The Journal of*

Experimental Biology, *224*(20). https://doi.org/10.1242/JEB.242300

Oulhen, N., Heyland, A., Carrier, T. J., Zazueta-Novoa, V., Fresques, T., Laird, J., Onorato, T. M., Janies, D., & Wessel, G. (2016). Regeneration in bipinnaria larvae of the bat star *Patiria miniata* induces rapid and broad new gene expression. *Mechanisms of Development*, *142*, 10–21. https://doi.org/10.1016/j.mod.2016.08.003

Özpolat, B. D., & Bely, A. E. (2016). Developmental and molecular biology of annelid regeneration: a comparative review of recent studies. *Current Opinion in Genetics & Development*, *40*, 144–153. https://doi.org/10.1016/j.gde.2016.07.010

Özpolat, B.D., Sloane, E.S., Zattara, E.E., and Bely, A.E. (2016) Plasticity and regeneration of gonads in the annelid *Pristina leidyi*. *EvoDevo* 7 (22). https://doi.org/10.1186/s13227-016-0059-1

Pernet, B., Amiel, A., & Seaver, E. C. (2012). Effects of maternal investment on larvae and juveniles of the annelid *Capitella teleta* determined by experimental reduction of embryo energy content. *Invertebrate Biology*, *131*(2), 82–95. https://doi.org/10.1111/j.1744-7410.2012.00263.x

Phipps, L. S., Marshall, L., Dorey, K., & Amaya, E. (2020). Model systems for regeneration: *Xenopus*. *Development (Cambridge)*, *147*(6). https://doi.org/10.1242/DEV.180844/223048

Planques, A., Malem, J., Parapar, J., Vervoot, M., & Gazave, E. (2019) Morphological, cellular and molecular characterization of posterior regeneration in the marine annelid *Playnereis dummerilli*. *Developmental Biology* 445(189-210). http://doi.org/10.10106/j.ydbio.2018.11.004

Rawls, A., & Olson, E. N. (1997). *MyoD* meets its maker. *Cell*, *89*(1), 5–8. https://doi.org/10.1016/S0092-8674(00)80175-0

Schindelin, J., Arganda-Carreras, I., Frise, E., Kaynig, V., Longair, M., Pietzsch, T., Preibisch, S., Rueden, C., Saalfeld, S., Schmid, B., Tinevez, J. Y., White, D. J., Hartenstein, V., Eliceiri, K., Tomancak, P., & Cardona, A. (2012). Fiji: an open-source platform for biological-image analysis. *Nature Methods 2012 9:7*, *9*(7), 676–682. https://doi.org/10.1038/nmeth.2019

Schoeman, S., & Simon, C.A. (2023). Live to die another day: regeneration in *Diopatra aciculata* Knox and Cameron, 1971 (Annelida: Onuphidae) collected as bait in Knysna Estuary, South Africa. *Biology*. 12(3), 483. https://doi.org/10.3390/biology12030483

Seaver, E. C. (2022). Sifting through the mud: a tale of building the annelid *Capitella teleta* for EvoDevo studies. *Current Topics in Developmental Biology*, *147*, 401–432. https://doi.org/10.1016/BS.CTDB.2021.12.018

Seaver, E. C., Thamm, K., & Hill, S. D. (2005). Growth patterns during segmentation in the two polychaete annelids, *Capitella* sp. I and *Hydroides elegans*: comparisons at distinct life history stages. *Evolution Development*, *7*(4), 312–326. https://doi.org/10.1111/j.1525-142X.2005.05037.x

Singer, M. (1954). Induction of regeneration of the forelimb of the postmetamorphic frog by augmentation of the nerve supply. *Journal of Experimental Zoology*, *126*(3), 419–471. https://doi.org/10.1002/jez.1401260304

Stewart, B. (1998). Sub-lethal predation and rate of regeneration in the euryalinid snake star *Astrobrachion constrictum* (Echinodermata, Ophiuroidea) in a New Zealand fiord. *Journal of Experimental Marine Biology and Ecology*. 199(2), 269-283. https://doi.org/10.1016/0022-0981(95)00177-8

927 Sur, A., Magie, C. R., Seaver, E. C., & Meyer, N. P. (2017). Spatiotemporal regulation of nervous system
928 development in the annelid *Capitella teleta*. *8*, 13. https://doi.org/10.1186/s13227-017-0076-8

929 Vickery, M.S., McClinktock, J.B. (1998). Regeneration in metazoan larvae. *Nature*. 394, 140.
930 https://doi.org/10.1038/28086

931 Vickery, M. C. L., Vickery, M. S., Amsler, C. D., & McClintock, J. B. (2001). Regeneration in echinoderm
932 larvae. *Microscopy Research and Technique*, *55*(6), 464–473. https://doi.org/10.1002/jemt.1191

933 Vickery, Minako S., Vickery, M. C. L., & McClintock, J. B. (2002). Morphogenesis and organogenesis in the
934 regenerating planktotrophic larvae of asteroids and echinoids. *Biological Bulletin*, *203*(2), 121–133.
935 https://doi.org/10.2307/1543381

936 Wilhelm, E., Bückmann, D., & Tomaschko, K.H. (1997). Life cycle and population dynamics of
937 *Pycnogonum litorale* (Pycnogonida) in a natural habitat. Marine Biology 129, 601–606.
938 https://doi.org/10.1007/s002270050202

939 Yamaguchi, E., Dannenberg, L. C., Amiel, A. R., & Seaver, E. C. (2016). Regulative capacity for eye
940 formation by first quartet micromeres of the polychaete *Capitella teleta*. *Developmental Biology*,
941 *410*(1), 119–130. https://doi.org/10.1016/j.ydbio.2015.12.009

942 Yamaguchi, E., & Seaver, E. C. (2013). The importance of larval eyes in the polychaete *Capitella teleta*:
943 effects of larval eye deletion on formation of the adult eye. *Invertebrate Biology*, *132*(4), 352–367.
944 https://doi.org/10.1111/ivb.12034

945 Zammit, P. S. (2017). Function of the myogenic regulatory factors *Myf5*, *MyoD*, *Myogenin* and *MRF4* in
946 skeletal muscle, satellite cells and regenerative myogenesis. *Seminars in Cell & Developmental*
947 *Biology*, *72*, 19–32. https://doi.org/10.1016/J.SEMCDB.2017.11.011

948 Zattara, E. E., & Bely, A. E. (2013). Investment choices in post-embryonic development: quantifying
949 interactions among growth, regeneration, and asexual reproduction in the annelid *Pristina leidyi*.
950 *Journal of Experimental Zoology Part B: Molecular and Developmental Evolution*, *320*(8), 471–488.
951 https://doi.org/10.1002/jez.b.22523

952 Zattara, E. E., & Bely, A. E. (2016). Phylogenetic distribution of regeneration and asexual reproduction in
953 *Annelida*: regeneration is ancestral and fission evolves in regenerative clades. *Invertebrate Biology*,
954 *135*(4), 400–414. https://doi.org/10.1111/IVB.12151

955 Zattara, E.E. & Fernández-Alvarez, F.A. (2022) Collecting and culturing *Lineus sanguineus* to study
956 *Nemertea* WBR. In: Blanchoud S, Galliot B, editors. Whole-Body Regeneration: Methods and
957 Protocols [Internet]. New York (NY) Chapter 12. doi: 10.1007/978-1-0716-2172-1_12

958 Zattara E.E., Fernández-Álvarez F. A., Hiebert T. C., Bely A. E. & Norenburg J. L. (2019) A phylum-wide
959 survey reveals multiple independent gains of head regeneration in *Nemertea*. The Royal Society.
960 https://doi.org/10.1098/rspb.2018.2524

961 Zou, J., Wu, X., Shi, C., Zhong, Y., Yan, Q., Su, L., and Li, G. (2021) A potential method for rapid screening
962 of amphioxus founder harboring germline mutation and transgene. *Front. Cell Dev. Biol.* 9 (702290)
963 doi: 10.3389/fcell.2021.702290

964

965

966 **Figure Legends**

967 Figure 1. Larvae and regenerating juveniles of *C. teleta*. All images are oriented in ventral view with
968 anterior to the left. **A** Stage 6 larva. **B** Stage 9 larva. **C**, **D**, and **E** are images of the posterior end of a
969 regenerating juvenile 3 days post-amputation (dpa) and are from the same specimen. **C** Differential
970 interference contrast (DIC) image showing regeneration of new tissue in juveniles. **D** Nervous system
971 visualized with anti-acetylated tubulin antibody labeling. **E** Phalloidin staining shows muscle fibers with
972 few fibers in the regenerating tissue. The white dotted lines indicate amputation sites. The asterisk
973 marks the position of the mouth. N denotes the number of animals scored that resemble the image
974 shown. Cm, circular muscle; ey, eyes; g, gut; mg, midgut; np, neural projection; pt, prototroch; py,
975 pygidium; tt, telotroch.

976 Figure 2. Amputated larvae undergo successful wound healing. All images are oriented in ventral view
977 with anterior to the left. Arrows indicate the continuous layer of epithelium, indicative of successful
978 wound healing. **A** Stage 6 uncut larva showing experiment design for amputations. The dotted lines
979 indicate cut sites: (aa) anterior amputation and (pa) posterior amputation. **B** Stage 6 larva 6 hpa anterior
980 amputation. **C** Stage 6 larva 6 hpa posterior amputation. **D** Stage 9 larva 6 hpa posterior amputation. **E**
981 Stage 9 larva 2 dpa anterior amputation. **F** Larva 3 dpa anterior amputation. The black bracket
982 represents the tissue between the gut and ectoderm. Amputation site indicated by the black dotted line.
983 N denotes the number of animals scored that resembled the image in the panel. Scale bar is 50 µm.

984 Figure 3. Localized cell proliferation near the amputation site in larvae. All images are oriented in ventral
985 view with anterior to the left. Animals were exposed to EdU to label dividing cells. EdU+ cells are green.
986 **A–D** are uncut controls: **A** Stage 6, **B** Stage 7, **C** Stage 9, and **D** Stage 9 larvae. **E–H** are anterior
987 amputations: **E** 6 hpa, **F** 1 dpa, **G** 3 dpa, and **H** 5 dpa larvae. **I–L** are posterior amputations: **I** 6 hpa, **J** 1
988 dpa, **K** 3 dpa, and **L** 5 dpa larvae. **M**, **N** Quantification of EdU incorporation in anterior (M) and posterior
989 (N) amputations and comparison with uncut controls. Time after amputation is on the X-axis and the
990 ratio of EdU/DAPI cells is on the Y-axis. The white arrows indicate EdU+ cells near the wound site. The
991 developmental stage or time post-amputation is indicated in the bottom left corner of each panel. N
992 denotes the number of animals scored that resemble the image shown. Dark blue bars in the graphs
993 represent uncut controls and light blue bars represent amputated animals. Asterisk denotes significance
994 with $p < 0.05$. Ant amp, anterior amputation; Post amp, posterior amputation. Scale bar is 50 µm.

995 Figure 4. *Vasa* is expressed at the wound site in amputated larvae. All images are oriented in ventral
996 view with anterior to the left. The purple coloration indicates localization of *vasa* transcripts by in situ
997 hybridization. **A**, **B**, and **C** *Vasa* expression patterns in uncut larvae at Stage 6, Stage 8, and Stage 9. **D**, **E**,
998 and **F** are anterior larval amputations. **G**, **H**, and **I** are posterior larval amputations. **D** and **G** are
999 amputated larvae 6 hpa (D) and 2 hpa (**G**). **E** *De novo* expression is observed in anterior amputations at 2
1000 dpa, as indicated by the arrow and is no longer detectable by 5 dpa (**F**). In posterior amputations,
1001 expression near the wound site is observed at both 2 dpa (**H**) and 3 dpa (**I**), as indicated by arrows. The
1002 time post-amputation is indicated in the bottom left corner of each panel in D–I. N denotes the number
1003 of animals scored that resemble the image shown. Ant amp, anterior amputation; Fg, foregut; mpc,
1004 multi-progenitor cell cluster; Post amp, posterior amputation; pgz, posterior growth zone. Scale bar is 50
1005 µm.

1006 Figure 5. Tissue response to amputation. **A–C** and **F–I"** are oriented in ventral view. **C–D"** are oriented in
1007 lateral view. In all images, anterior is to the left. **A** uncut Stage 6 larva labeled with anti-acetylated
1008 tubulin to visualize the nervous system and ciliary bands. Larvae are labeled with anti-acetylated tubulin
1009 (red) and phalloidin (green) showing the nervous system and musculature for all panels except A, C and
1010 G. Larvae shown in panels A, C and G were labeled with anti-acetylated tubulin. **B** and **B'** are the same
1011 specimen 6 hpa. **C** neural fibers are present distal to the cut site in 2 dpa posterior amputee (arrow). **D**
1012 larva 6 hpa after anterior amputation. **E**, **E'** and **E"** are the same specimen, 3 dpa anterior amputation. **E'**
1013 magnified view of muscle fibers as marked by phalloidin. **E"** magnified view of anti-acetylated tubulin
1014 labeling. **F**, **F'**, and **F''** are the same larva 2 dpa. **F** Nervous system and musculature in a larva 2 dpa. **F'**
1015 magnified view of posterior wound site showing few muscle fibers distal to cut site. **F"** magnified view of
1016 posterior wound site showing fibers in the tissue distal to the amputation site (arrows). **G** shows a
1017 specimen lacking neural fibers distal to the cut site. **H**, **H'**, and **H"** are the same individual at 5 dpa
1018 posterior amputation. **H'** neurites distal to the cut site (arrow). **H''** longitudinal and circular muscles are
1019 present distal to the cut site (bracket). White brackets in H, **H'** and **H"** indicate tissue distal to the
1020 amputation site. N denotes the number of animals scored that resemble the representative image.
1021 Amputation site is indicated by a white dotted line. vnc, ventral nerve cord; pn, peripheral nerves. Scale
1022 bar is 50 µm.

1023 Figure 6. Amputation induces *ash1* but not *elav* expression at the anterior wound site. All images are
1024 oriented with anterior to the left. **A-E** are ventral views and **F-I** are lateral views. The purple coloration
1025 indicates expression of either *ash1* (**A-E**) or *elav* (**F-I**) transcripts. **C-E** and **H-I** are anterior amputations. **A**
1026 Stage 6 uncut control. **B** Stage 9 uncut control. **C** 6 hpa. **D** and **E** are the same 3 dpa individual. Vertical
1027 arrows indicate novel *ash1* ectodermal expression. The boundary between ectodermal and mesodermal
1028 layers is indicated by a black dotted line. **F** Stage 6 and **G** Stage 9 uncut controls. **H** 6 hpa. **I** 3 dpa. N
1029 denotes the number of animals scored that resemble the image indicated. Ant amp, anterior
1030 amputation; br, brain; fg, foregut; vnc, ventral nerve cord. Scale bar is 50 µm.

1031 Figure 7. Amputation induces expansion of *MyoD* expression. All images are oriented in ventral view
1032 with anterior to the left. Localization of *MyoD* transcripts is visualized by the purple coloration. **A** Stage 6
1033 and **B** Stage 9 uncut controls. *MyoD* is expressed in the posterior trunk mesoderm. **C** and **D** are anterior
1034 amputations (ant amp). **C** 6 hpa. **D** anterior shift of anterior boundary of *MyoD* expression is observed at
1035 7 dpa. **E** 6 hpa posterior amputation (post amp). Spots of staining anterior to the bracket is nonspecific
1036 trapping in the chaetae. **F** *MyoD* is expressed along the length of the body in 3 dpa animals (compare
1037 with E). Brackets indicate the regions of detectable *MyoD* expression along the anterior-posterior axis.
1038 Amputation sites are indicated by black dotted lines. N denotes the number of animals scored that
1039 resemble the representative image. Ant amp, anterior amputation; Post amp, posterior amputation.
1040 Scale bar is 50 µm.

1041 Figure 8. Rare eye reformation following anterior amputation. All images are oriented with anterior to
1042 the left. **A** – **D** are ventral views. **A** DIC image of the anterior end of a Stage 9 uncut larva. **B** DIC image of
1043 the anterior end of a larva 5 days after anterior amputation. The image shown is a merge of multiple
1044 focal planes. The pigmented cells (pc) of the eye are indicated by arrows. **C**–**F** eye sensory cells (sc, white
1045 arrows), labeled by the 22C10 antibody (green). **C** Uncut Stage 9 control. **D** anterior amputated larva 5
1046 dpa. **E** and **F** are juvenile worms in lateral view. **E** uncut 2 week-old juvenile and **F** juvenile 1 week post-
1047 amputation of the head. **G** Table displaying the number of pigment cells, sensory cells, or either cell

1048 (total) present in anteriorly amputated larvae at 6 hpa and 3 dpa or later. The dotted line indicates the
1049 outline of the animal. Juv, juvenile; mg, midgut; pc, pigment cells; sc, sensory cells.

1050 Figure 9. Rare reformation of cilia occurs in amputated larvae. Animals are labelled with anti-acetylated
1051 tubulin (white). All images are oriented in with anterior to the left. **A, C, E, B,** and **F** are oriented in
1052 lateral view. **B, D, G, H,** and **H'** are oriented in ventral view. **A** Stage 6 uncut larva. **D** Stage 9 uncut larva.
1053 **B** and **E** are anterior amputations. **B** larva 6 hpa. **E** larva 5 dpa with short cilia visible distal to the cut site
1054 (arrow). **D, H,** and **H'** are posterior amputations in ventral view. **D** larva 6 hpa. **H** and **H'** larva 5 dpa with
1055 both long cilia (LC) and short cilia (SC) distal to the cut site (arrows). **H'** is a magnification of **H**. N denotes
1056 the number of animals scored that are similar to the image represented. Amputation site is indicated by
1057 the white dotted line. Ant amp, anterior amputation; lc, long cilia; nt, neurotroch; post amp, posterior
1058 amputation; pt, prototroch; pyg, pygidium; sc, short cilia; tt, telotroch. Scale bar is 50 µm.

1059 Figure 10. Induction of metamorphosis in amputated larvae. All images are oriented in ventral view with
1060 anterior to the left. **A** Uncut Stage 9 larva. **B** Uncut animal 2 hr after induction with metamorphic cue. **C**
1061 anteriorly amputated larva not exposed to metamorphic cue. **D** anteriorly amputated animal 2 hr after
1062 exposure to metamorphic cue. **E** posteriorly amputated larva not exposed to metamorphic cue. **F**
1063 posteriorly amputated animal 2 hr after exposure to metamorphic cue. N denotes the number of
1064 animals scored that are similar to the image shown. Ant amp, anterior amputation; Br, brain; ph,
1065 pharynx; post amp, posterior amputation; pt, prototroch; tt, telotroch. All images have the same
1066 magnification; scale bar, 50 µm.

1067

1068

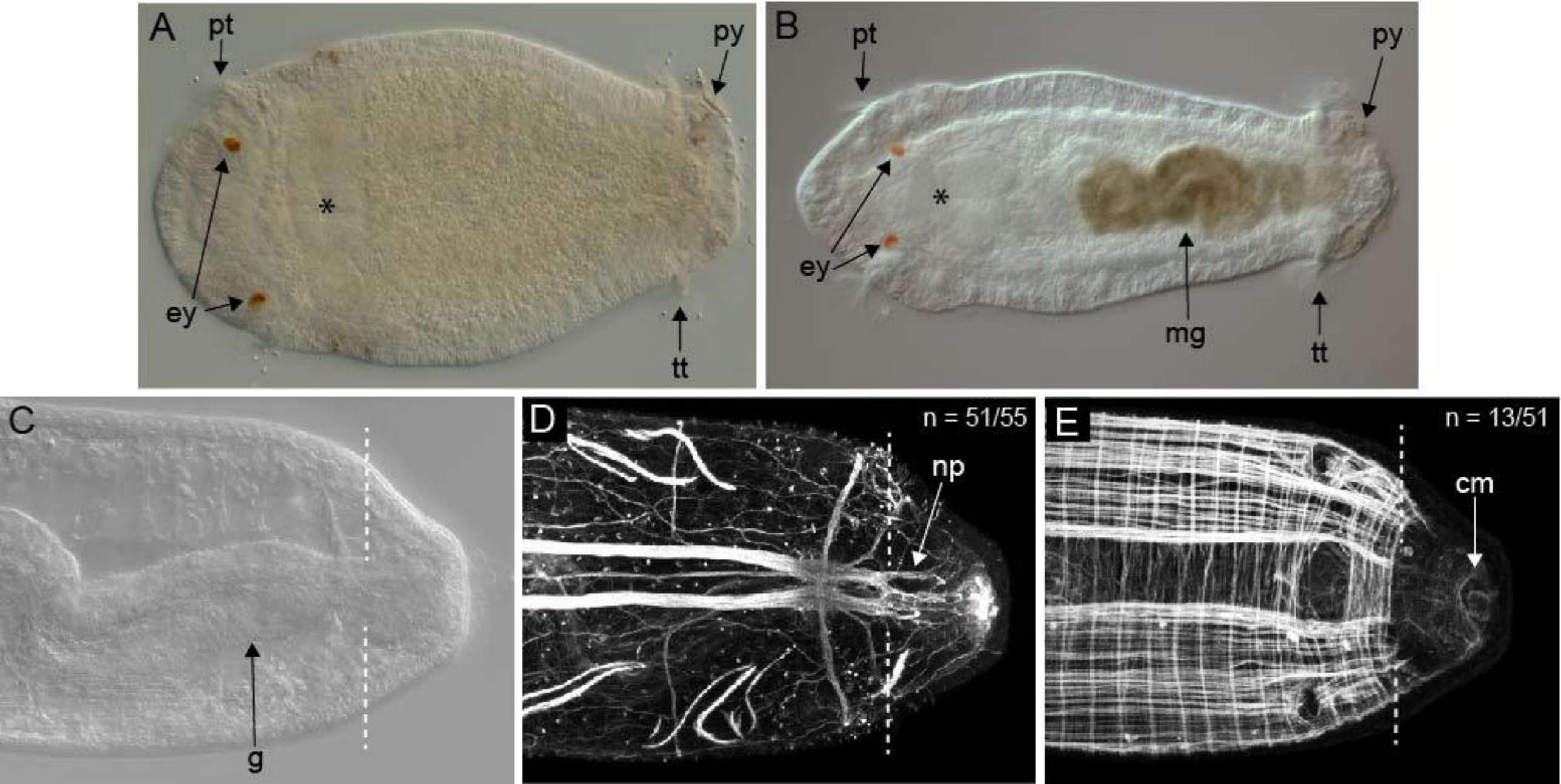
A
pt
py
ey
*
tt
B
pt
py
ey
*
mg
tt
C
g
D
n = 51/55
np
E
n = 13/51
cm

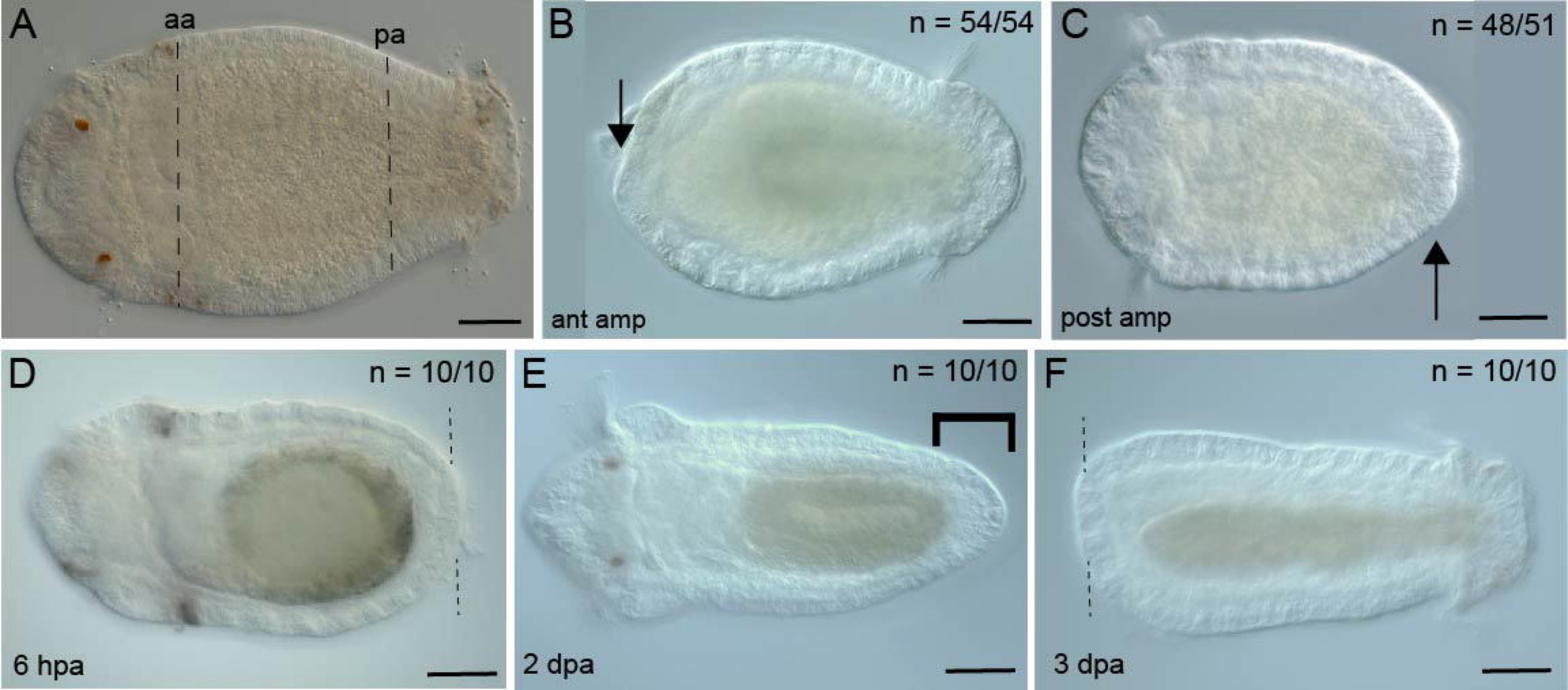
A
aa
pa
B
n = 54/54
ant amp
C
n = 48/51
post amp
D
n = 10/10
6 hpa
E
n = 10/10
2 dpa
F
n = 10/10
3 dpa

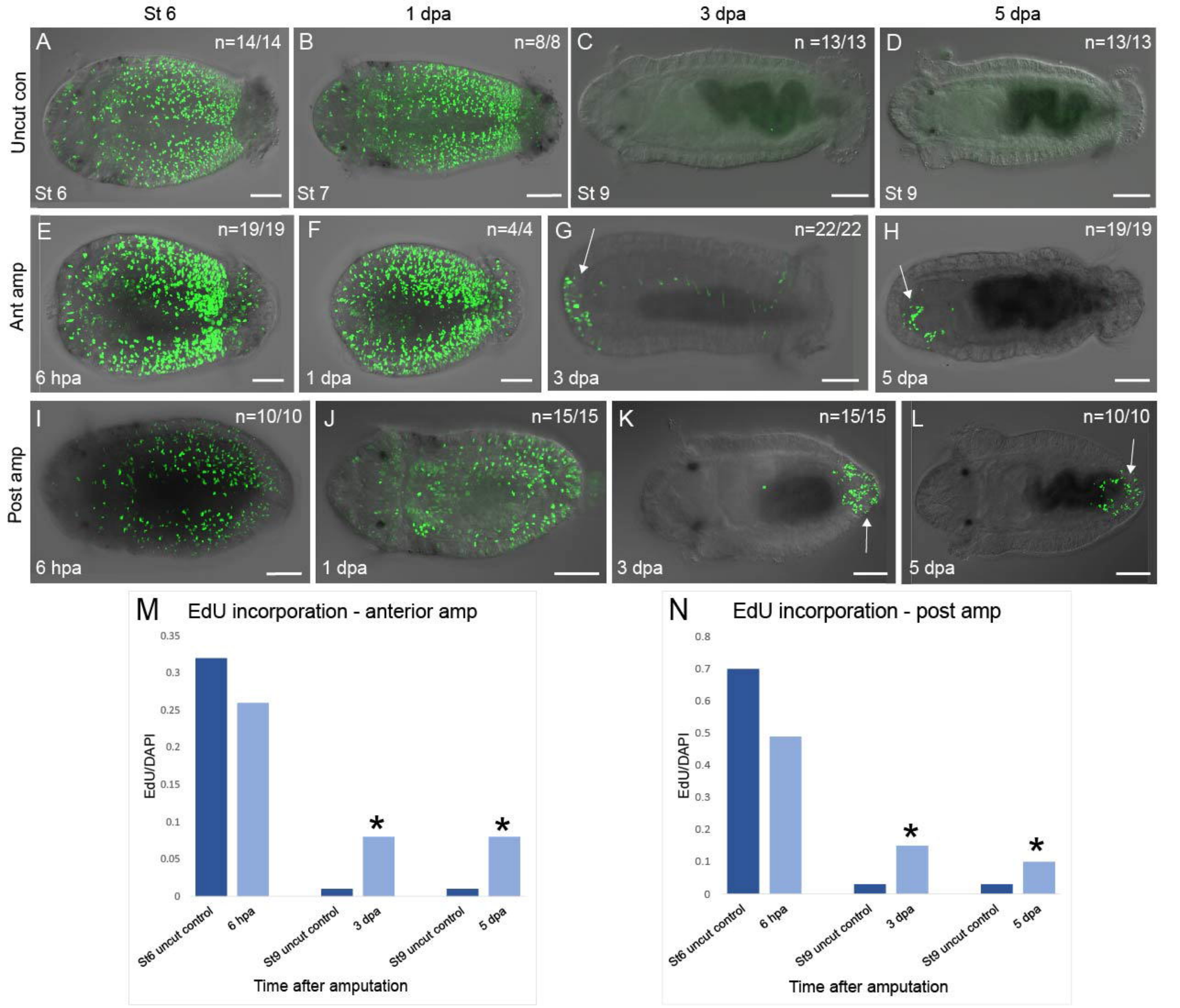
St 6
1 dpa
3 dpa
5 dpa
Uncut con
Ant amp
Post amp
A
n=14/14
St 6
B
n=8/8
St 7
C
n =13/13
St 9
D
n=13/13
St 9
E
n=19/19
6 hpa
F
n=4/4
1 dpa
G
n=22/22
3 dpa
H
n=19/19
5 dpa
I
n=10/10
6 hpa
J
n=15/15
1 dpa
K
n=15/15
3 dpa
L
n=10/10
5 dpa
M
EdU incorporation - anterior amp
EdU/DAPI
0.35
0.3
0.25
0.2
0.15
0.1
0.05
0
*
*
St6 uncut control
6 hpa
St9 uncut control
3 dpa
St9 uncut control
5 dpa
Time after amputation
N
EdU incorporation - post amp
EdU/DAPI
0.8
0.7
0.6
0.5
0.4
0.3
0.2
0.1
0
*
*
St6 uncut control
6 hpa
St9 uncut control
3 dpa
St9 uncut control
5 dpa
Time after amputation

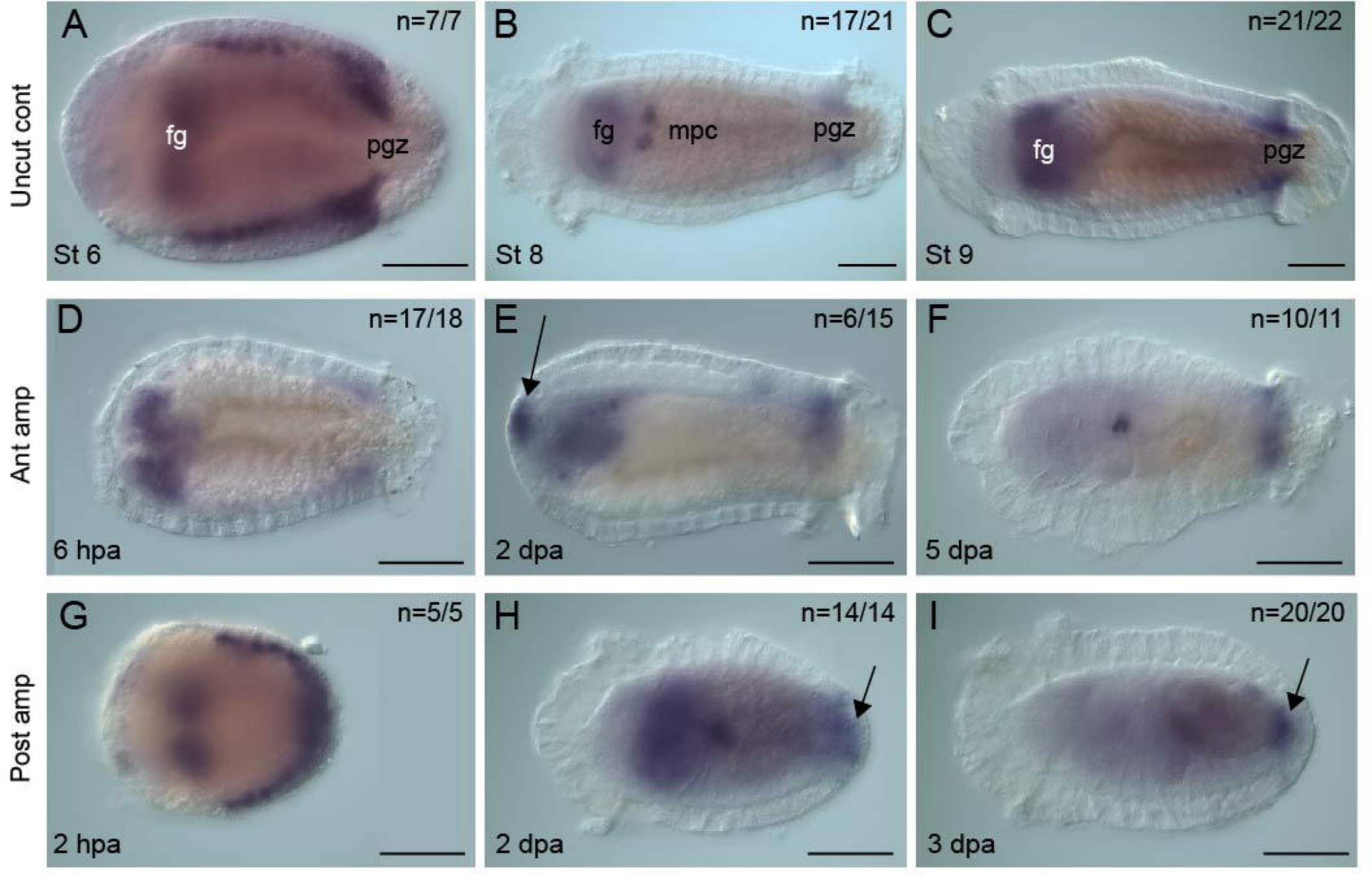
Uncut cont
Ant amp
Post amp
A
n=7/7
fg
pgz
St 6
B
n=17/21
fg
mpc
pgz
St 8
C
n=21/22
fg
pgz
St 9
D
n=17/18
6 hpa
E
n=6/15
2 dpa
F
n=10/11
5 dpa
G
n=5/5
2 hpa
H
n=14/14
2 dpa
I
n=20/20
3 dpa

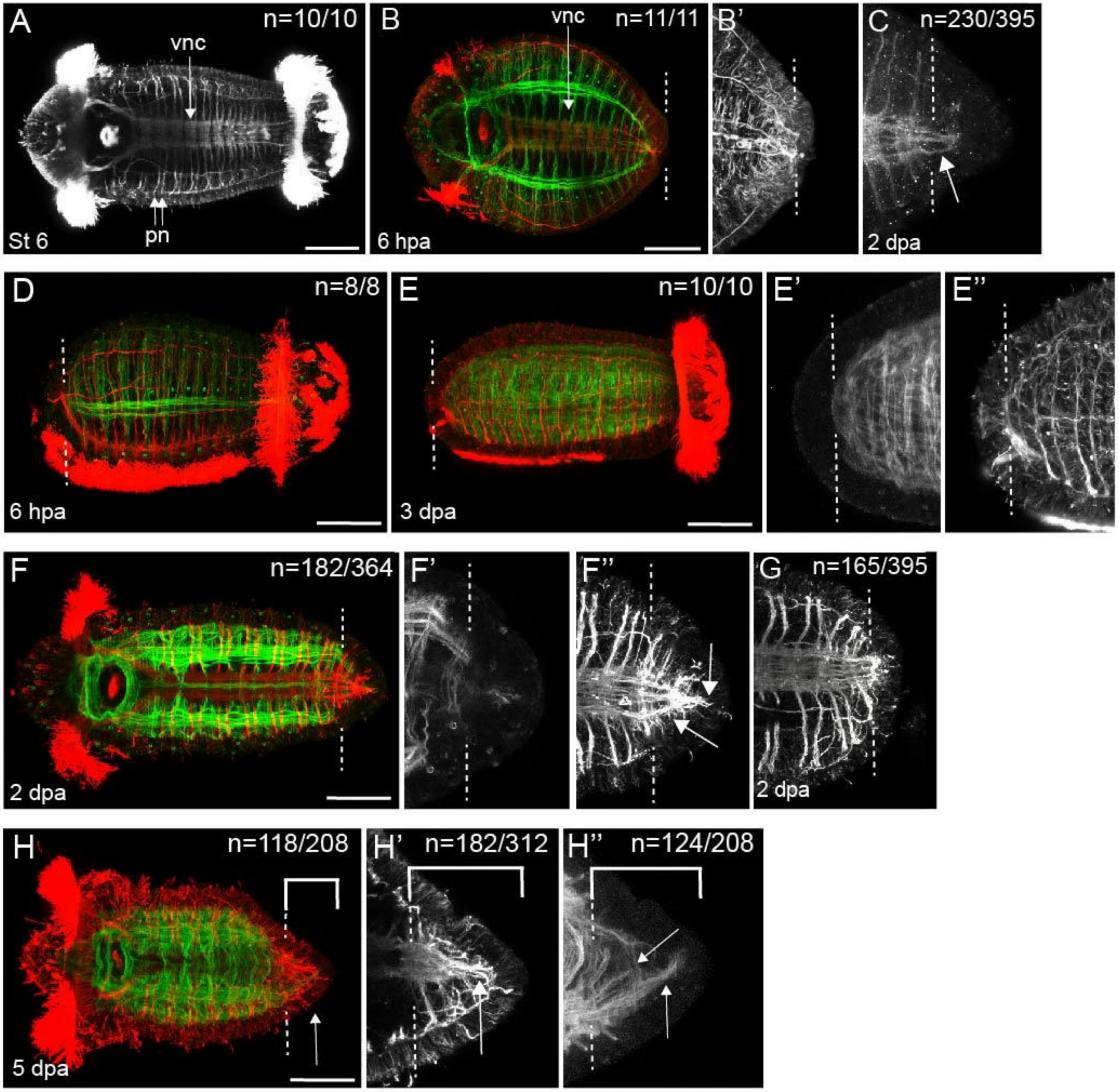
A
n=10/10
vnc
pn
St 6
B
vnc
n=11/11
6 hpa
B'
C
n=230/395
2 dpa
D
n=8/8
6 hpa
E
n=10/10
3 dpa
E'
E''
F
n=182/364
2 dpa
F'
F''
G
n=165/395
2 dpa
H
n=118/208
5 dpa
H'
n=182/312
H''
n=124/208

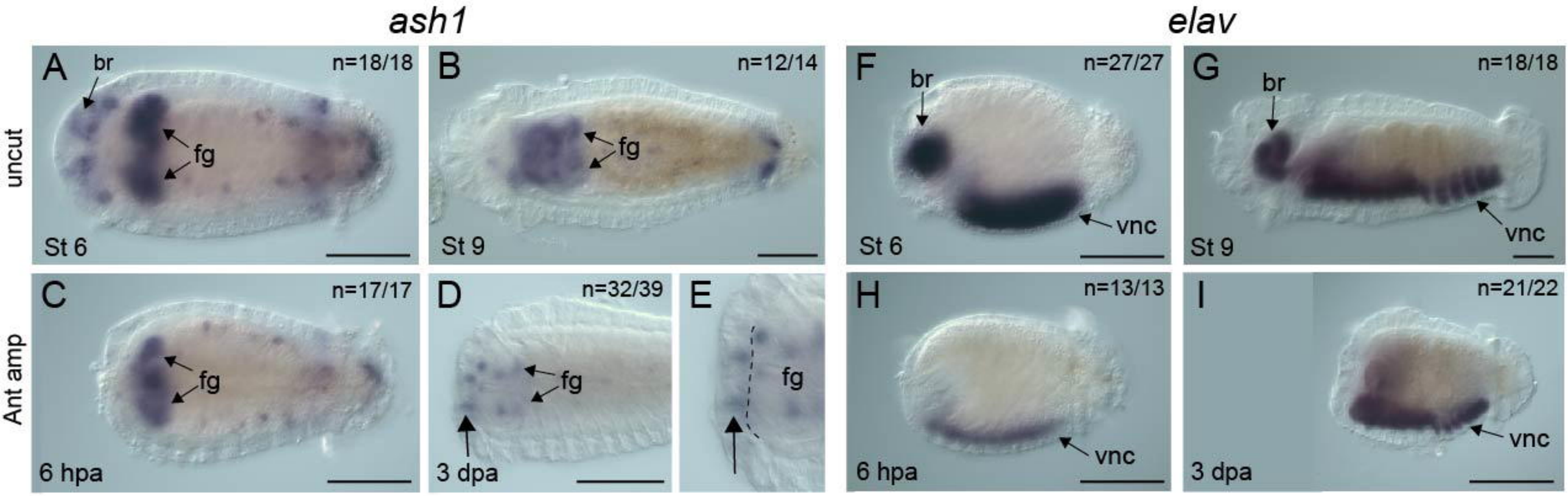
ash1
elav
uncut
Ant amp
A
br
fg
n=18/18
St 6
B
fg
n=12/14
St 9
F
br
vnc
n=27/27
St 6
G
br
vnc
n=18/18
St 9
C
fg
n=17/17
6 hpa
D
fg
n=32/39
3 dpa
E
fg
H
vnc
n=13/13
6 hpa
I
vnc
n=21/22
3 dpa

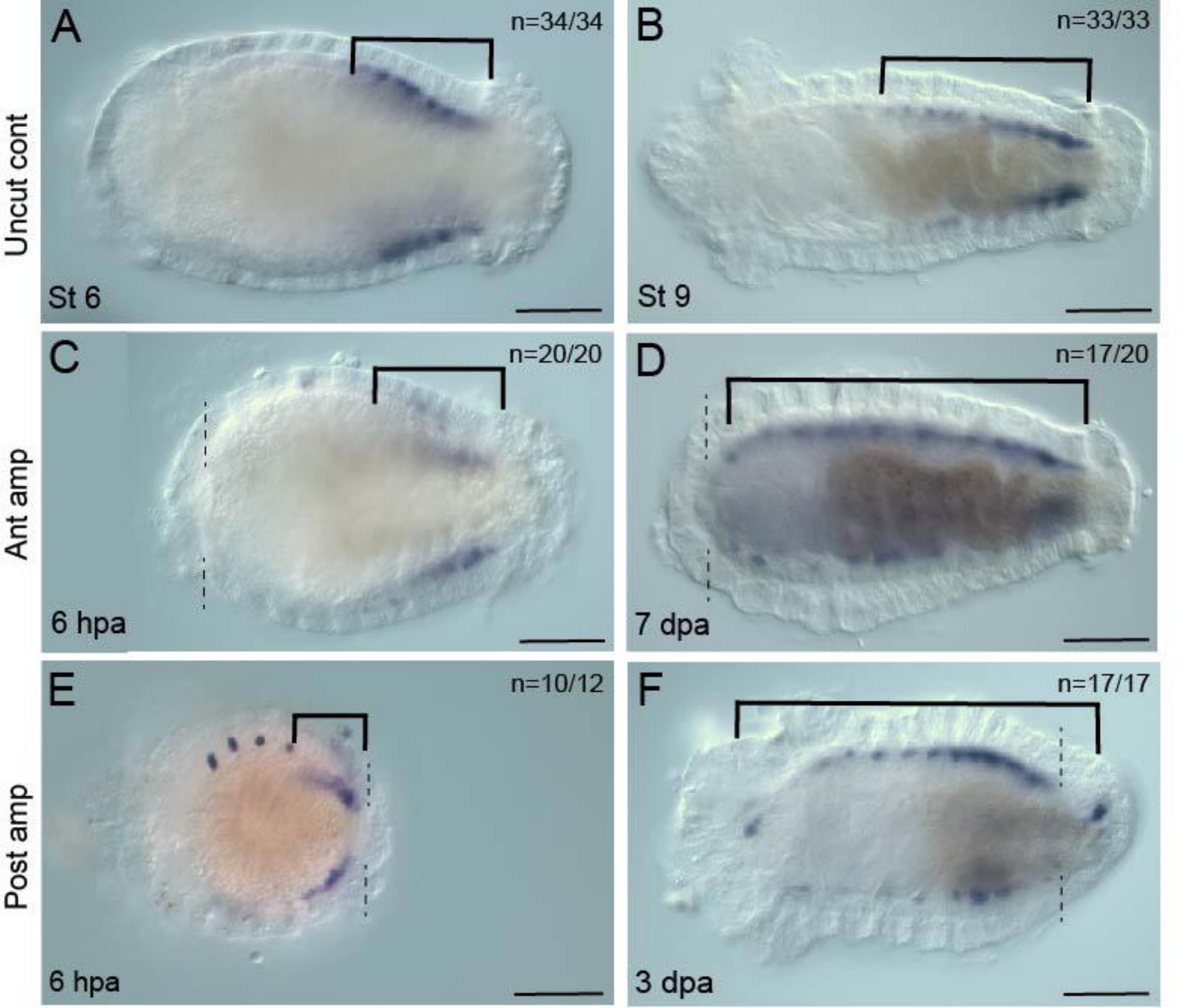
A
n=34/34
St 6
B
n=33/33
St 9
C
n=20/20
6 hpa
D
n=17/20
7 dpa
E
n=10/12
6 hpa
F
n=17/17
3 dpa
Uncut cont
Ant amp
Post amp

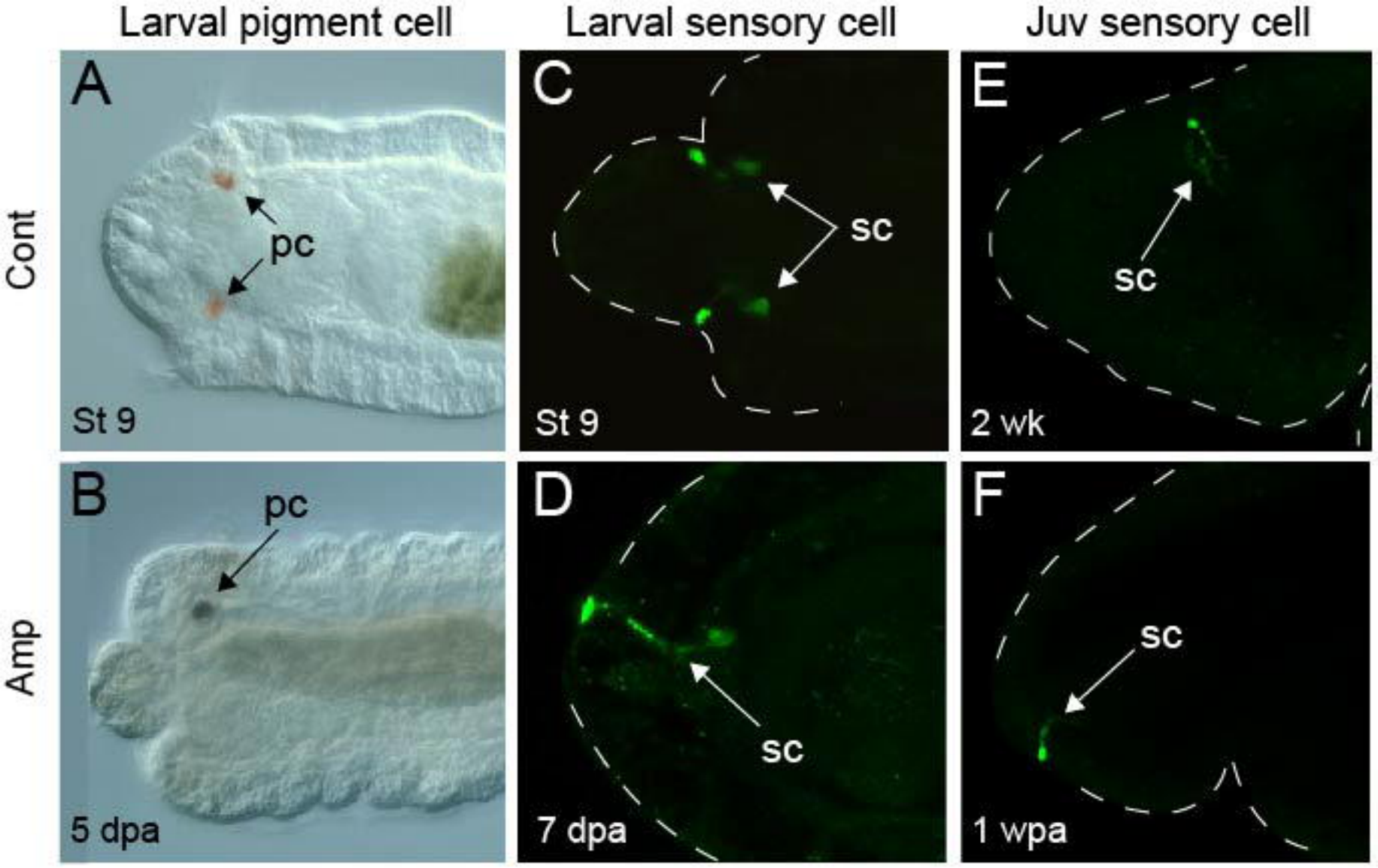

G

	Pigment cell	Sensory cell	Total
6 hpa	0/46	0/31	0/57
3 dpa +	28/420	8/220	36/640
	7%	4%	6%

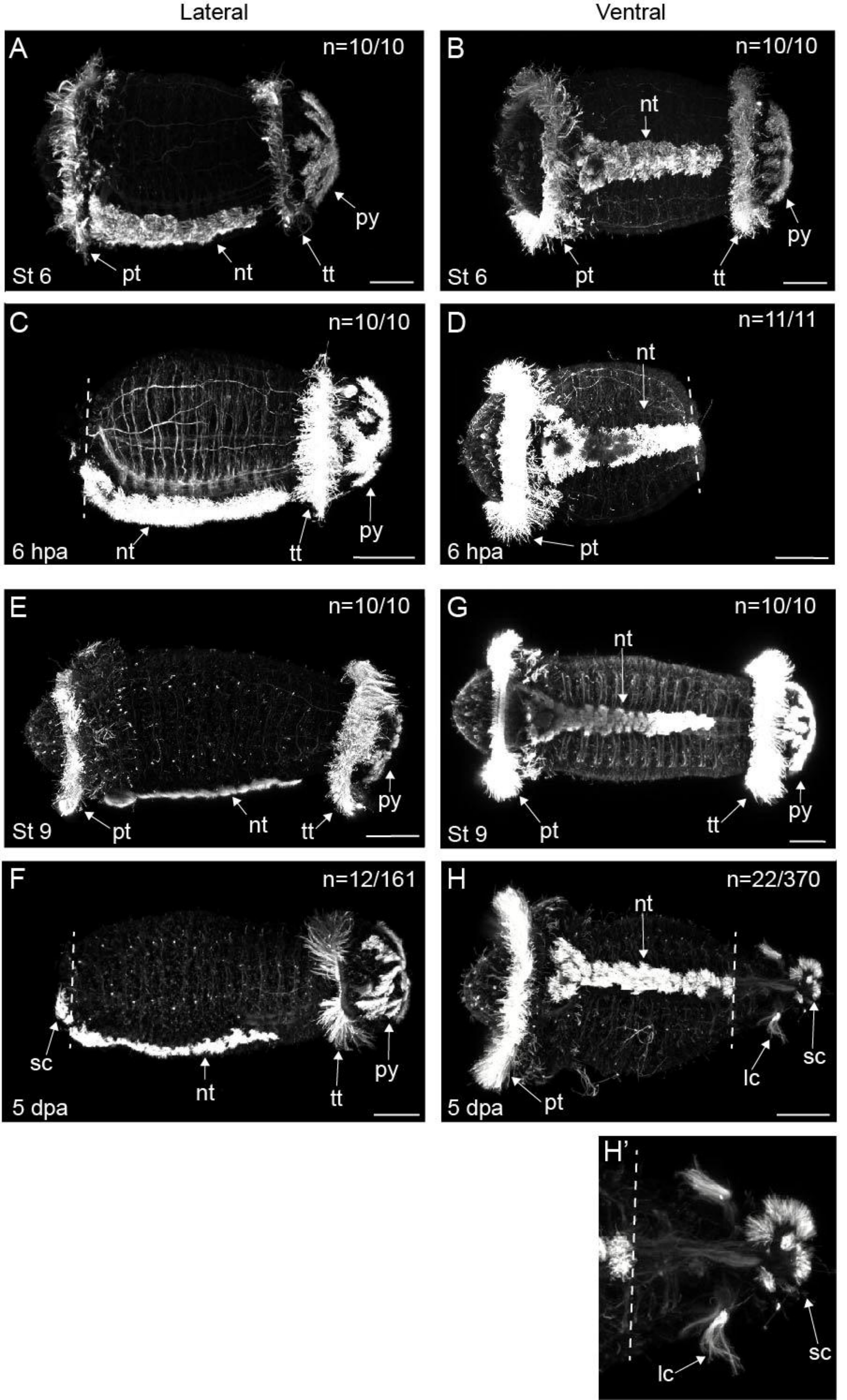
Lateral
Ventral
A
n=10/10
St 6
pt
nt
tt
py
B
n=10/10
St 6
nt
pt
tt
py
C
n=10/10
6 hpa
nt
tt
py
D
n=11/11
6 hpa
nt
pt
E
n=10/10
St 9
pt
nt
tt
py
G
n=10/10
St 9
nt
pt
tt
py
F
n=12/161
5 dpa
sc
nt
tt
py
H
n=22/370
5 dpa
nt
pt
lc
sc
H'
lc
sc

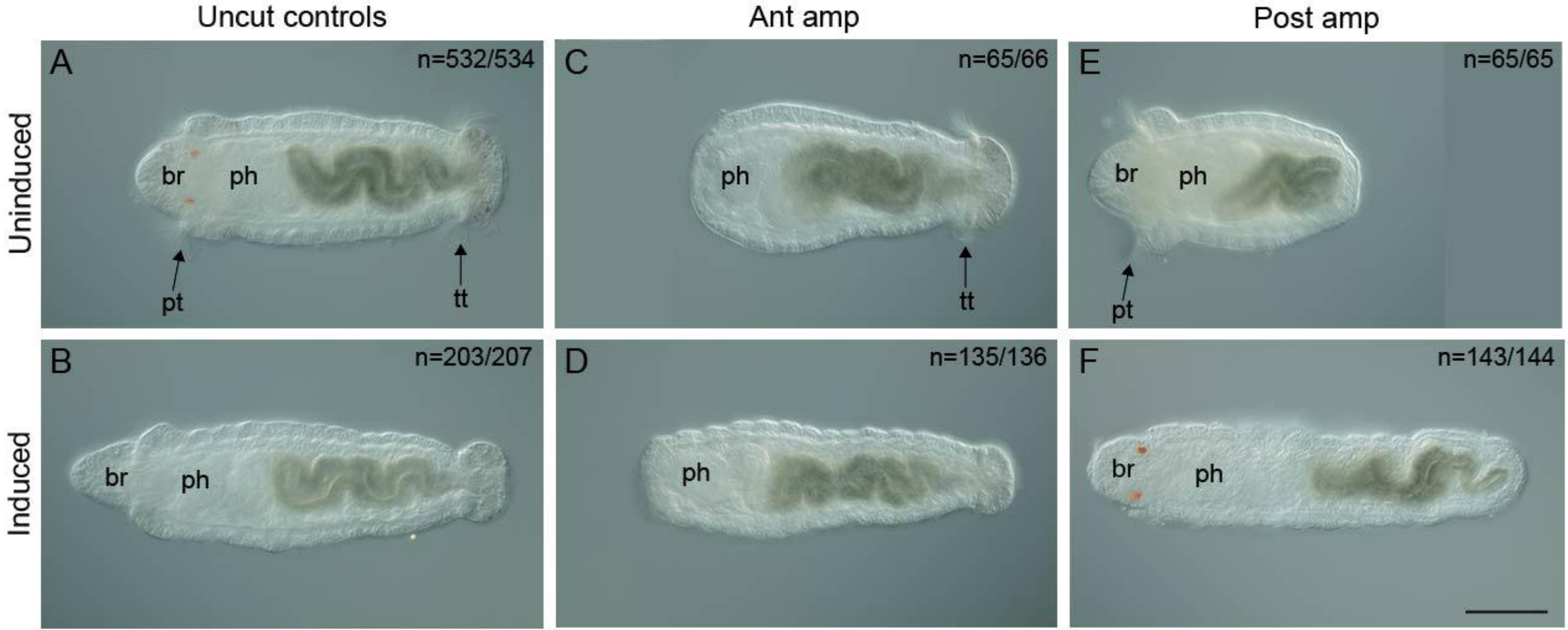
Uncut controls
Ant amp
Post amp
Uninduced
Induced
A
n=532/534
br
ph
pt
tt
C
n=65/66
ph
tt
E
n=65/65
br
ph
pt
B
n=203/207
br
ph
D
n=135/136
ph
F
n=143/144
br
ph

Table 1. Mean values of EdU+ cells in anterior amputations

Anterior Amp		**Anterior**		**Middle**		**Posterior**	
		Uncut	**Cut**	**Uncut**	**Cut**	**Uncut**	**Cut**
6 hpa	**# EdU**	133	102	466	235	387	136
	# Nuclei	418	392	1216	417	551	250
	%	32%	26%	38%	56%	70%	54%
3 dpa	**# EdU**	3	29	18	2	14	24
	# Nuclei	447	363	856	457	413	185
	%	1%	8%	2%	0%	3%	13%
5dpa	**# EdU**	3	28	18	5	14	10
	# Nuclei	147	359	856	516	413	219
	%	2%	8%	2%	1%	3%	5%

Table 2. Mean of EdU+ cells in posterior amputations

Posterior Amp		**Anterior**		**Middle**		**Posterior**	
		Uncut	**Cut**	**Uncut**	**Cut**	**Uncut**	**Cut**
6 hpa	**# EdU**	133	70	466	217	387	225
	# Nuclei	418	155	1216	556	551	463
	%	32%	45%	38%	39%	70%	49%
3 dpa	**# EdU**	3	2	18	6	14	78
	# Nuclei	447	306	856	702	413	525
	%	1%	1%	2%	1%	3%	15%
5dpa	**# EdU**	3	0	18	0	14	51
	# Nuclei	147	331	856	547	413	513
	%	2%	0%	2%	0%	3%	10%

Table 3. Measurement of tissue distal to cut site

		Muscle	Nervous System	Gut	Width 2 /Width 1
Ant Amp	**6 hpa**	19 µm	18 µm	N/A	N/A
	3 dpa	22 µm	15 µm	N/A	N/A
Post Amp	**6 hpa**	* 17 µm	* 12 µm	N/A	0.675
	5 dpa	* 62 µm	* 67 µm	* 45 µm	0.453
	St 9 6 hpa	N/A	N/A	* 37 µm	N/A

* = significance, $p < .05$